Chemical Engineering Science 192 (2018) 993–1010

Contents lists available at ScienceDirect

Chemical Engineering Science

journal homepage: www.elsevier.com/locate/ces

Interface evolution of a liquid Taylor droplet during passage through a sudden contraction in a rectangular channel

T. Sudhakar [a,b], Arup Kumar Das [b,*]

[a] National Institute of Technology Uttarakhand, Srinagar (Garhwal), Uttarakhand, India
[b] IIT Roorkee, Roorkee, Uttarakhand, India

HIGHLIGHTS

- Lattice approach has been presented for handling complex interfacial interaction.
- Evolution of liquid-liquid interface while passing through restriction has been studied.
- Droplet bypass through symmetric and asymmetric contractions are simulated.
- Reducing the contraction ratio offers more resistance to the droplet.
- With inclination of channel, time span for passage of the restriction decreases.

ARTICLE INFO

Article history:
Received 26 April 2018
Received in revised form 11 July 2018
Accepted 9 August 2018
Available online 10 August 2018

Keywords:
Lattice Boltzmann
Interface
Evolution
Contraction
Orifice

ABSTRACT

A lattice Boltzmann discretization based numerical study has been carried out to study the effect of sudden contraction in a rectangular channel during uprise of a lighter liquid species inside a heavier one. Diffused interface concept has been adopted for the prediction of liquid-liquid interface. Simulations are performed for passage of a kerosene droplet through restrictions like a sudden contraction, orifice, and remotely spaced contraction-expansion. A wide range of contraction ratio, droplet volume, and channel inclinations are considered to study the evolution of interface along the rectangular conduit. Symmetric change of interfacial shape has been observed while droplet tries to accommodate in the narrow confined zone after contraction. Using streamlines and velocity vectors, the reasons behind the interfacial evolution are established. With a decrease in contraction ratio, resistance against droplet passage increases this produces lengthier lamella like kerosene interface in the downstream of contraction. Droplet volume showed a significant effect in constructing the tail interfacial structure, which allows water to penetrate inside kerosene core for larger volumes. During the passage of a kerosene droplet in a channel with different inclination, stage of an asymmetric interface is observed. By providing offset contraction, local asymmetries are observed in the kerosene interface near the plane of area reduction. Efforts are continued to observe the kerosene droplet passage through an orifice which showed restricted and free interfacial evolution after contraction and expansion sections, respectively. The stabilizing zone between contraction and expansion showed influence on the generation of daughter droplets by fragmenting kerosene interface.

1. Introduction

Flow of two different phases or components inside channels having geometrical singularity is quite common in industrial applications. Nuclear, oil exploration, refineries, chemical reactors are examples exhibiting passage of interfacial entity through contraction, expansion or bend planes. At the plane of singularity, interface reorients from stable shape to accommodate the progressive change of forces and then finally equilibrates. Study of dynamic change in interface shape is essential as the evolution of phase boundary alters mass, momentum and energy transfer across it. Passage of gaseous phase through sudden change in conduit cross-section leads to pressure drop of the flow which has been determined by researchers (Janssen and Kervinen, 1964; Geiger, 1964; Chisholm, 1968; Weisman et al., 1976; Gnglielmini et al., 1986; Schmidt and Friedel, 1997; Attou et al., 1997; Mandal et al. (2008); Miqdad et al. (2016)) using careful experimentation. With the industrial revolution in this century, pipe fittings became

* Corresponding author.
E-mail addresses: sudhakar@nituk.ac.in (T. Sudhakar), akdasfme@iitr.ac.in (A.K. Das).

https://doi.org/10.1016/j.ces.2018.08.024
0009-2509/

essential and researchers felt a need to study in the direction of two phase flow through sudden geometry modifications. Abdelall et al. (2005) extended work from the previous century and proposed a correlation for pressure drop in small and mini channels having a sudden contraction. On a similar note, Chen et al. (2008) have also proposed a pressure drop correlation for contraction in a rectangular channel to circular one carrying air-water two phase flow. Balakhrisna et al. (2010) have studied experimentally, the effect of sudden contraction and expansion in liquid-liquid interaction for different types of flow patterns. Sadatomi et al. (2013) visualized flow pattern in air-water combination for a wide range of Reynolds number through contraction, expansion and bend sections. Padilla et al. (2013) carried forward the work for refrigerant as a working fluid and proposed that sudden acceleration in contraction section is responsible for frictional pressure drop. Kawahara et al. (2015) have studied the effect of contraction ratio using different liquids and complemented the study by careful numerical investigation using volume of fluid method. Still a thorough knowledge of interfacial evolution while passing through a restriction in the flow path is still due. Present paper targets fundamental understanding of interface evolution of a droplet in the stages of approach, passing by and departure through flow restrictions using numerical simulation.

With the increase of computational facility and development of robust numerical models, the study of the phenomenon with complex physics and domain became a trend. In the effort of utilizing efficient model framework, newer techniques like smoothed particle hydrodynamics (Das and Das, 2010), molecular dynamics (Ansari et al., 2016) are becoming popular beside well established Eulerian volume of fluid method. These new microscale methodologies are Lagrangian in nature and have limitations in terms of memory while modeling engineering scale geometries. To bridge the gap between classical control volume based scheme and efficient microscopic methods, efforts are being made to device mesoscopic techniques. Lattice Boltzmann method (Succi et al., 1993) is one such development which became popular for having better connectivity with neighboring lattices than conventional finite volume method. Simulations of typical two phase flow using the lattice Boltzmann method is becoming popular amongst researchers (Zou and He, 1997; Zheng et al., 2006). Ghosh et al. (2012) have studied the dynamics of Taylor bubble by varying inclination of the channel, bubble volume and channel geometry using lattice Boltzmann method. But the study of complex dynamics of an interface while traversing through sudden contraction and expansion with asymmetry and different channel inclinations is still dew. In this paper, using the lattice Boltzmann method, an effort has been made to understand such interface evolutions. Next section discusses the model framework using lattice structure in brief and describes the generalized domain considered for the present study.

2. Model development

Mesoscopic, three-dimensional Lattice Boltzmann method is used for tracking the dynamic nature of the liquid-liquid interface. D3Q19 lattice arrangement and possible directions of propagation of physical information are used for discretizing the domain. A representative lattice and its directional nomenclature system have been shown in Fig. 1(a). For studying flow dynamics of kerosene droplet passing through a restriction in a conduit filled with water, a domain consisting of three separate segments is chosen. The bottom most portion of the domain can be called as droplet developing section having W_1 X W_1 square cross-section and L_1 length. A droplet of the lighter liquid has been initially placed in this section and allowed to move up by virtue of gravity ($g\sin\theta$; θ is the inclination angle of the domain with horizontal). L_1 has been chosen based on the volume of the droplet to be accommodated. At the top most portion of the developing section, another segment having W_2 X W_2 passageway for a span of L is interconnected. With the consideration of $W_2 < W_1$, this section can be called as contraction zone. Eccentricity due to center lines of the developing and contraction zone is considered as 'e' which can be tuned to a non-zero value for getting an asymmetric arrangement of a sudden change in the cross-sectional plane. Third and last segment of the domain (W_3 X W_3 X L_3) is placed on top of the contraction zone to allow the restoration of the deformed interface. $W_3 = W_2$ has been considered for getting a domain of simple contraction. Apart from the common portions of the faces, rest surfaces are considered to have no slip and no penetration boundary conditions. A schematic diagram of the domain has been shown in Fig. 1(b).

Flow in this domain will be associated with two fluids, having different densities, represented as ρ_l and ρ_h for low and high density fluids respectively. To represent the bulk behavior and capture the features near interface separately, two derived properties are defined as:

$$n = \frac{\rho_i + \rho_j}{2}$$
$$\phi = \frac{\rho_i - \rho_j}{2} \tag{1}$$

Here, ρ_i and ρ_j are the individual phase densities which can be ρ_h and ρ_l or any other intermediate value depending on the initial condition of the domain.

Phase continuity and momentum equations can be re-casted using concept of n and ϕ to average out the bulk behavior and highlight interfacial dynamics. It needs to be mentioned that interdependence between the constitutive equations is maintained based on fundamental physics. The functional forms of the equations are as follows (Zheng et al., 2006):

$$\frac{\partial n}{\partial t} + \vec{\nabla} \cdot (n\vec{u}) = 0 \tag{2}$$

$$\frac{\partial (n\vec{u})}{\partial t} + \vec{\nabla} \cdot (n\vec{u}\vec{u}) = -\phi\vec{\nabla}\mu_\phi - \vec{\nabla}p_o + \mu_\phi\vec{\nabla}\phi + \vec{F}_b + \vec{\nabla} \cdot (\mu\vec{\nabla}\vec{u}) \tag{3}$$

$$\frac{\partial \phi}{\partial t} + \vec{\nabla} \cdot (\phi\vec{u}) = \vec{\nabla} \cdot (\theta_M\vec{\nabla}\mu_\phi) \tag{4}$$

where μ_ϕ is chemical potential, θ_M is mobility of fluid, $\vec{F_b}$ is body force and p_o is pressure tensor.

Chemical potential for liquid-liquid interfacial behavior and mobility can be calculated from interface thickness and surface tension (Ghosh et al., 2012).

To discretize the governing Eqs. (2)–(4), Boltzmann approximation is used and two probability distribution functions, $f_i(\vec{x}, t)$ and $g_i(\vec{x}, t)$, are defined. The distribution function $g_i(\vec{x}, t)$ is allotted to replicate the interface dynamics. The relation between ϕ and $g_i(\vec{x}, t)$ can be derived from probabilistic summation in all possible directions as (Zheng et al., 2006):

$$\phi = \sum_i g_i \tag{5}$$

Lattice structures interact among themselves through the stages of collision and streaming. Chaotic collision kinetics can be simplified using linear averaging within single relaxation time (τ_ϕ). Using BGK model after Bhatnagar, Gross and Krook invention, lattice collisions can be linked up with departure from equilibrium. Immediately followed by collision stages, lattice information are

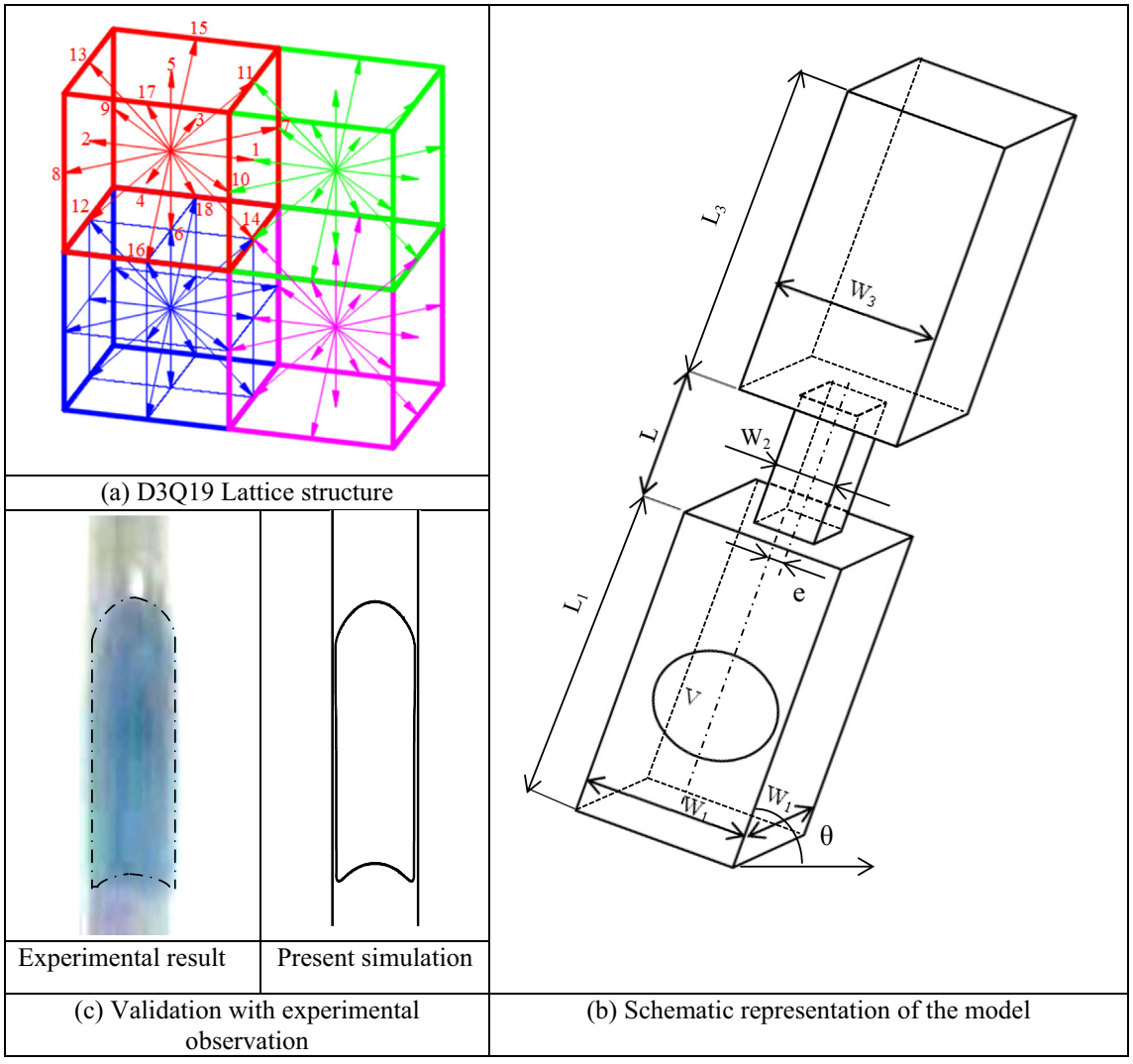

Fig. 1. (a) Demonstration of D3Q19 Lattice structure with nomenclature; (b) description of domain and definition of physical variables; (c) validation of developed code with in-house experimental results for kerosene–water Taylor droplet in a channel.

streamed in predefined directions as per the chosen framework. Both the phenomenon can be cumulatively expressed in terms of probability distribution function, $g_i(\vec{x},t)$ as:

$$g_i(\vec{x}+\vec{e}_i\Delta t, t+\Delta t) = g_i(\vec{x},t) + \frac{g_i^{(eq)}(\vec{x},t) - g_i(\vec{x},t)}{\tau_\phi} \tag{6}$$

Here, $\vec{e}_i$ is the lattice velocity vector and $g_i^{(eq)}(\vec{x},t)$ is the equilibrium function which can be derived from Maxwell-Boltzmann equilibrium distribution as:

$$g_i^{(eq)}(\vec{x},t) = A_i + B_i\phi + C_i\phi\,\vec{e}_i\cdot\vec{u} \tag{7}$$

To replicate the interface equilibrium behavior based on factor for restraining mobility (Γ), the coefficients in Eq. (9) are considered as:

$$\begin{aligned} A_i &= -3\Gamma\mu_\phi \\ B_i &= 1,\ B_i = 0\ (i \neq 1) \\ C_i &= \frac{1}{2q} \end{aligned} \tag{8}$$

Here, q is the control parameter for computation and linked up with relaxation time (τ_ϕ) as:

$$q = \frac{2}{2\tau_\phi + 1} \tag{9}$$

It is to be noted that the adopted single relaxation time method is prone to have numerical instabilities for high Reynolds number ($Re = \frac{\rho_h u_{TB} D}{\mu} > 200$) flow (Yu and Fan, 2010). But for the problems simulated in present effort, we have dealt with liquid-liquid system having maximum Re in the range of 65 (<200). For these stable cases, reported in the next section, single relaxation is preferred above higher level relaxation based corrections (Aslan et al., 2014).

On the other hand, bulk behavior of the fluids in lattice framework is expressed in terms of n which can be found from a directional average of probability distribution function, $f_i(\vec{x},t)$. Eqs. (12) and (13) express the way of coupling between macroscopic properties n and velocity, u with mesoscopic probability distribution function, $f_i(\vec{x},t)$ as:

$$n = \sum_i f_i \tag{10}$$

$$u = \left(\sum_i f_i\vec{e}_i + \frac{1}{2}(\mu_\phi\nabla\vec{\phi} + \vec{F}_b)\right) \Big/ n \tag{11}$$

Similar to $g_i(\vec{x},t)$, following the stages of collision and streaming, a lattice Boltzmann equation can be formed to implement the continuity and momentum conservation (Eqs. (2) and (3)). In terms of probability distribution function, $f_i(\vec{x},t)$ it can be written as:

$$f_i(\vec{x}+\vec{\mathbf{e}}_i\delta_t, t+\delta_t) = \left(1-\frac{1}{\tau_\rho}\right)f_i(\vec{x},t) + \frac{f_i^{eq}(\vec{x},t)}{\tau_\rho} + \left(1-\frac{1}{2\tau_\rho}\right)\frac{w_i}{c_s^2}\left(\vec{\mathbf{e}}_i - \vec{u} + \frac{\vec{\mathbf{e}}_i\vec{u}}{c_s^2}e_i\right)(\mu_\phi\nabla\phi + F_B)\delta t \tag{12}$$

where equilibrium distribution function f_i^{eq} is expressed in terms of macroscopic velocities as:

$$f_i^{eq}(\vec{x},t) = w_i A_i + w_i n\left(3e_{i\alpha}u_\alpha - \frac{3}{2}u^2 + \frac{9}{2}u_\alpha u_\beta e_{i\alpha}e_{i\beta}\right) \tag{13}$$

Here, the constants can be expressed as:

$$A_1 = \left(\frac{9}{4}n\right) - \frac{15\left(\phi\mu_\phi + \frac{1}{3}n\right)}{4}$$
$$A_{i=2,\ldots,19} = 3\left(\phi\mu_\phi + \frac{1}{3}n\right) \tag{14}$$

Weightage of information flow in different lattice directions is expressed as:

$$w_1 = \frac{1}{3},\ w_{i=2,\ldots,7} = \frac{1}{18},\ w_{i=8,\ldots,19} = \frac{1}{36} \tag{15}$$

τ_ρ is the dimensional relaxation parameter which can be related to viscosity as:

$$\mu = c_s^2(\tau_\rho - 0.5)n \tag{16}$$

where $c_s = 1/\sqrt{3}$.

Modified bounce back condition (Ghosh et al., 2012) is used at the walls to provide no slip and no penetration condition. Itemized collision and forcing in the boundary nodes are used to ensure minimization of tangential flux along the wall (Meng et al., 2018). Present approach enforces opposite corner nodes to be also equal along with orthogonal and tangential directions.

Experimentally, an uprise of the liquid-liquid interface for a kerosene droplet in the stagnant water along the rectangular conduit has been captured. To validate the developed code using the model framework stated earlier, a numerical simulation has been performed for kerosene droplet in water along a rectangular conduit (10 mm × 10 mm). Interface shape of the Taylor droplet obtained numerically is compared with in-house experimental result. Snaps of the kerosene droplet are taken in an indigenously developed,

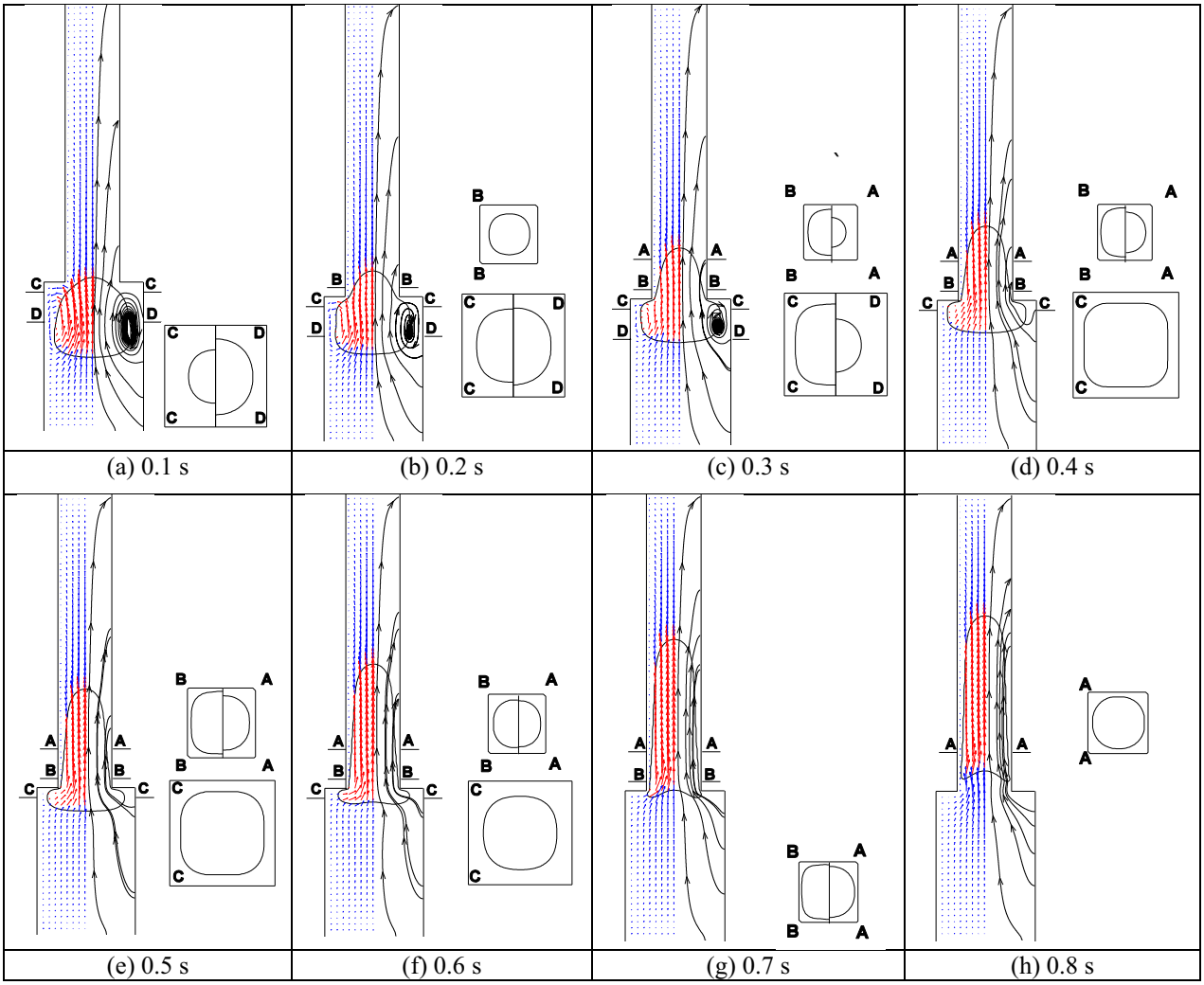

Fig. 2. Evolution of liquid-liquid interface during passage of a contraction plane in vertical configuration; Lateral view of droplet movement is shown with interface contour superposed with velocity vectors and streamlines in complimentary halves; complete or semi cross-sectional profiles (AA, BB, CC and DD) are shown in respective figures for comparison of shapes at different planes.

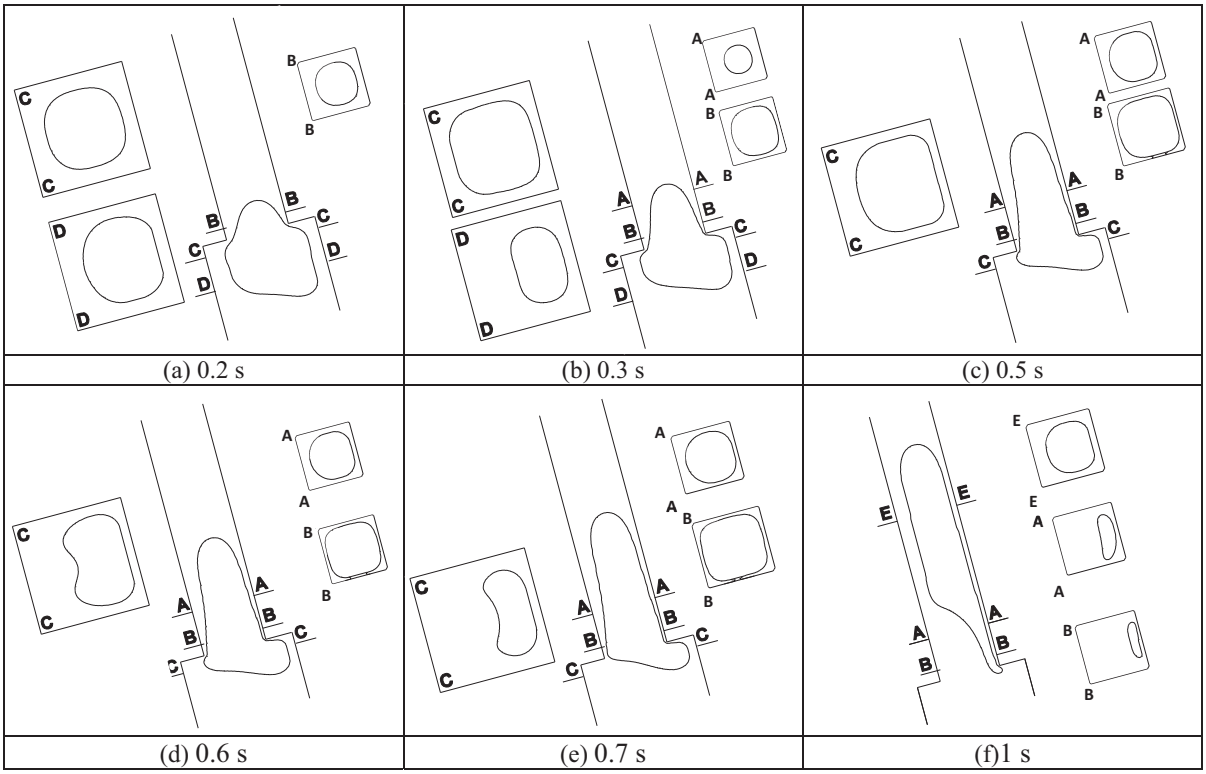

Fig. 3. Incurring asymmetry across the center line of rectangular channel having symmetric contraction but 75° inclined orientation. Lateral view of temporal droplet movement is shown with interface contour at different cross-sectional planes (AA, BB, CC, DD and EE).

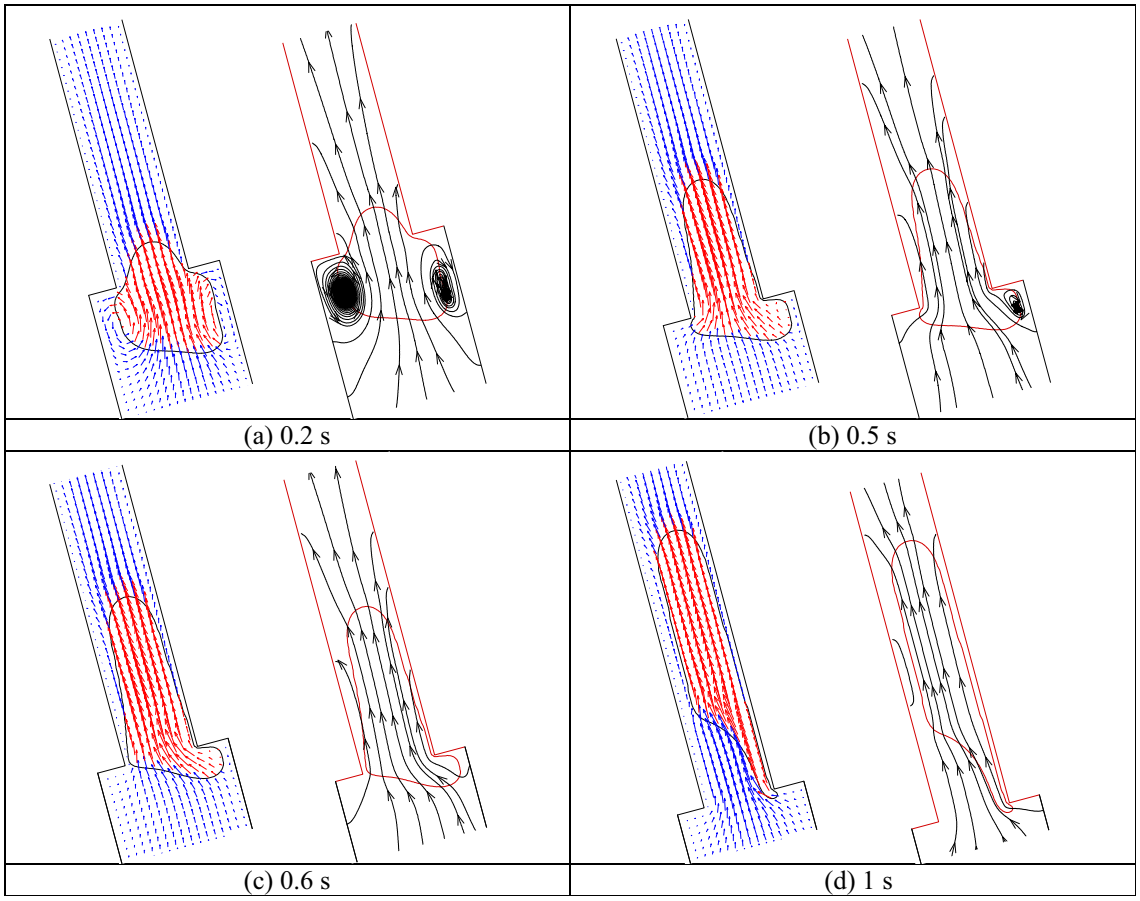

Fig. 4. Explanation of flow physics highlighting reasons behind asymmetry; velocity vectors and streamlines are plotted side by side at four different time intervals.

acrylic glass made a setup using high resolution camera (Canon EOS 5DS) at a frame rate of 20 shots/s. Side by side representation of the experimental screenshot and present numerical simulation is shown in Fig. 1(c). In this comparison, all parameters are kept similar. A good match in results between experimental and developed numerical model shows the ability of lattice Boltzmann framework for prediction of liquid-liquid interface. In the next section, we have demonstrated the results of numerical simulation related to kerosene droplet passage through the sudden restriction.

3. Results and discussion

3.1. Kerosene droplet passage through contraction inside conduit

At first numerical simulation is performed to observe the evolution of interfacial configuration while a kerosene droplet faces a sudden contraction during its uprise. Due to obstruction in its flow path, droplet adjusts its interfacial configuration for obtaining least resistant in upward motion. It will be interesting to note the transformation of shape from the numerical simulation performed in 3D lattice framework as described above. Representative snapshots of simulation have been tabulated in Fig. 2 for a droplet rise having Eötvös number $\left(Eo = \frac{\Delta\rho g D^2}{\sigma}\right)$ 50. Contraction ratio (W_2/W_1) has been kept as 0.5 and $W_2 = W_3$ is considered for modification of generalized domain to a channel having 1:4 area contraction at mid plane. The conduit has been kept as vertical having $\theta = 90°$. In Fig. 2, symmetric shape of the interface in longitudinal view has been utilized and both velocity vectors and streamlines of the complementary half domain are shown side by side. Cross-sectional interface configurations are also shown at several planes along with the longitudinal view to highlight the volumetric interfacial evolution process. During its uprise through larger cross-sectional area ($W_1 \times W_1$) kerosene droplet takes a spherical cap shape and progresses towards contraction plane. Water passes around the droplet through the annular film and allows the droplet to move up. Motion of the droplet becomes retarded as it reaches near the contraction plane due to resistance in its free rise. To accommodate with the sudden change in cross-sectional area kerosene–water interface reorients and the reason behind it can be clearly observed from the circulation at the bottom corner of the contraction plane. Pointed face of the droplet in comparison to its tail end, as observed at t = 0.1 s, has been resulted in the lesser area occupied by kerosene in plane CC (near to contraction plane) than DD (far away from contraction plane). Evolution of kerosene–water interface in the domain of lower cross-sectional (W_2 X W_2) area, above contraction plane has been observed at t = 0.2 s. Finite area occupied by kerosene in cross-sectional view near and downstream of contraction plane confirms entry of kerosene droplet. Circulation below the contraction plane feeds the developing kerosene droplet in smaller cross-sectional conduit consuming lighter phase from bottom part of the conduit. As the time progresses, droplet continues to elongate in the conduit after contraction plane. Around 0.5 s, a slender kerosene Taylor droplet can be observed in smaller diameter conduit, still receiving feed from the bottom. Subsequent comparison between two cross-sectional planes above

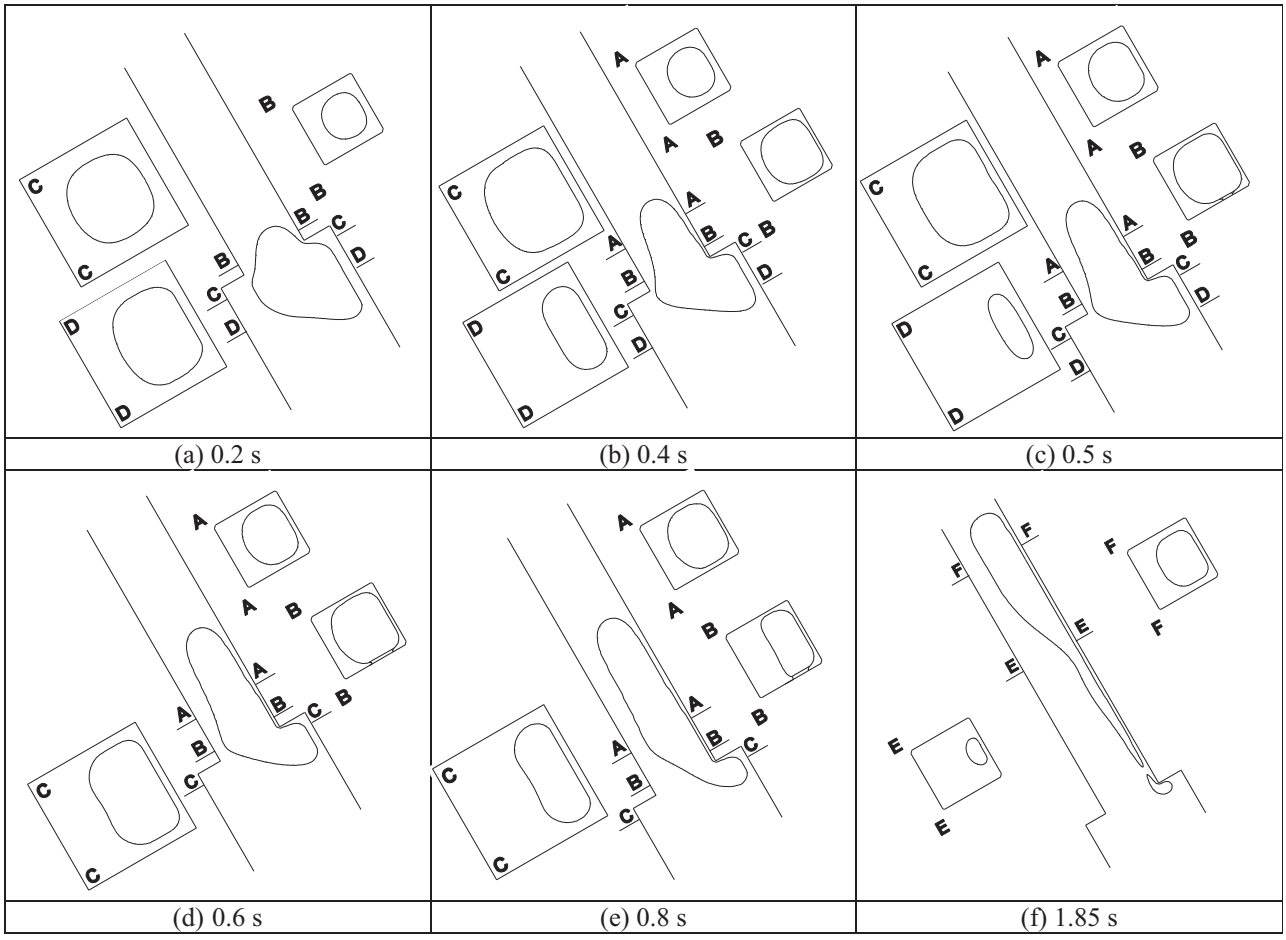

Fig. 5. Demonstration of increased asymmetry for a kerosene droplet passing through symmetric contraction but 60° inclined orientation. Lateral view of temporal droplet movement is shown with interface contour at different cross-sectional planes (AA, BB, CC, DD, EE and FF).

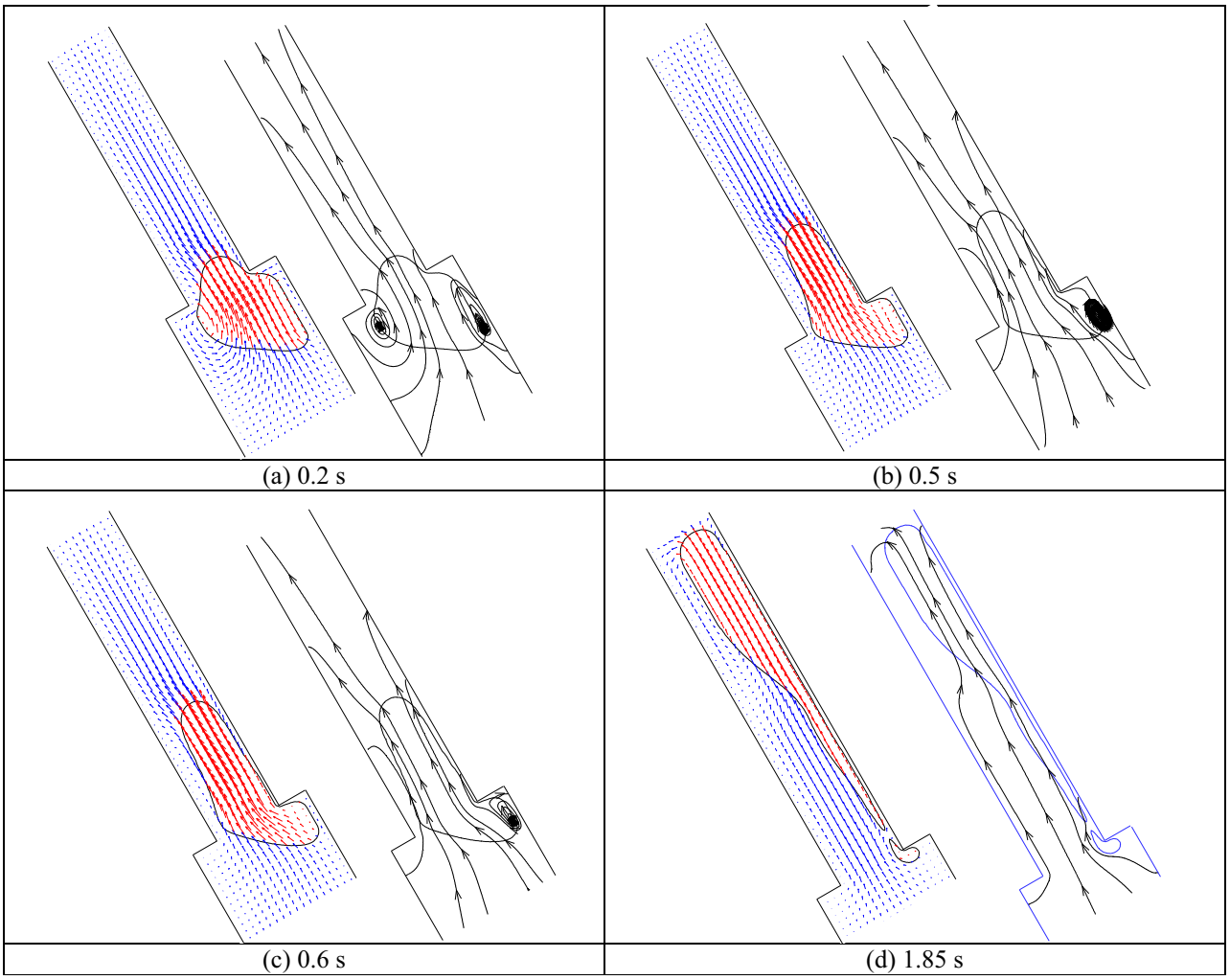

Fig. 6. Reasons behind asymmetry movement of droplet in 60° inclined channel having symmetric contraction; velocity vectors and streamlines explains flow physics around formation of daughter droplet.

the contraction zone depicts progressive area filling nature of Taylor droplet. At around 0.7 s, droplet completely passes the contraction plane to move upward as a whole in the form of a Taylor droplet. Similar cross-sectional areas are obtained as Taylor droplet has an asymptotic, long tail shape. In this zone, one can observe parallel velocity field or streamlines inside the droplet pushing it in upward direction. Present demonstration of droplet passage through a contraction plane clearly establishes the evolution of interface shape from spheroid cap to Taylor droplet. It is to be noted that the passage of a liquid droplet inside another liquid has not kept any residue in the contraction plane and not prone to form satellite at the tail of Taylor droplet.

This is to be noted that the simulation reported in Fig. 2 only handled transformation of symmetric interface posing a line of symmetry at the middle of symmetric contraction planes. Passage of a droplet through symmetric contraction plane inside an inclined conduit will be also interesting to observe which is expected to reorient interface differently as compared to a vertical one (reported in Fig. 2). Due to preferential gravity pull, droplet will deviate from the symmetric shape and stick with the upper wall even in the channel of constant cross-section (Bhusan et al., 2009).

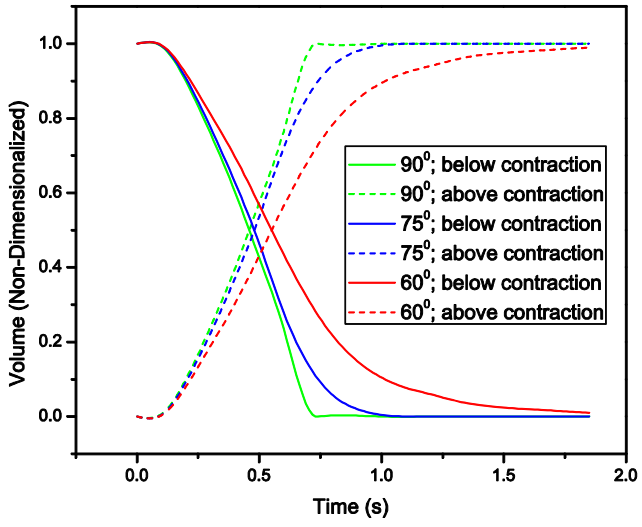

Fig. 7. Volume of droplet present above and below the contraction for different inclinations of channel; present figure represents droplet passage span for different inclinations.

3.2. Asymmetric droplet passage through contraction inside inclined conduit

Next numerical snapshots are depicted to explain stages behind the evolution of asymmetric interface, passing through the contraction. At first, simulation results are reported in Fig. 3, in which a kerosene droplet passing through a contraction plane inside 75° inclined conduit with horizontal. Temporal sequences clearly depict asymmetry along the center line of the channel. Lateral views depict the tendency of the droplet to stick with the upper side of the wall and hence generates asymmetric configuration while passing through the contraction plane.

Asymmetry initiates even in approach stage (Fig. 3(a)) and continues through offset evolution of interface in lower cross-sectional area (Fig. 3(b)) part of the channel. Though asymmetry is not prompt in near planes (BB and CC) of the contraction zone, it becomes noticeable while the droplet moves away from the sudden contraction (AA and DD). Developing droplet shifts towards upper face of the smaller sectional plane and blossoms further. In this process, kerosene inventory at the bottom side of the contraction plane gets consumed keeping larger protrusion in the right hand side of the lateral symmetry plane (Fig. 3(c),)d)). In the migration process of the kerosene phase, inside the smaller cross-sectional area (Fig. 3(e), (f)), an elongated Taylor droplet can be seen numerically having non-uniform film thickness around. Taylor droplet, adhered with the upper wall, shows larger asymmetry in the nose (section EE) zone while differential film thickness can be also observed in the elongated tail. Both velocity vectors and streamlines are presented in Fig. 4 to support occurrence of variation in strength of circulation and asymmetry in the droplet shape.

Asymmetric nature of droplet passage through contraction plane becomes more prompt for lower inclination of the conduit from horizontal. Effort has been made to observe the extent of asymmetry of the droplet for a wide range of inclination angle. As a representation, next, we present simulation results for 60° inclination with horizontal. Azimuthal asymmetry in the film can

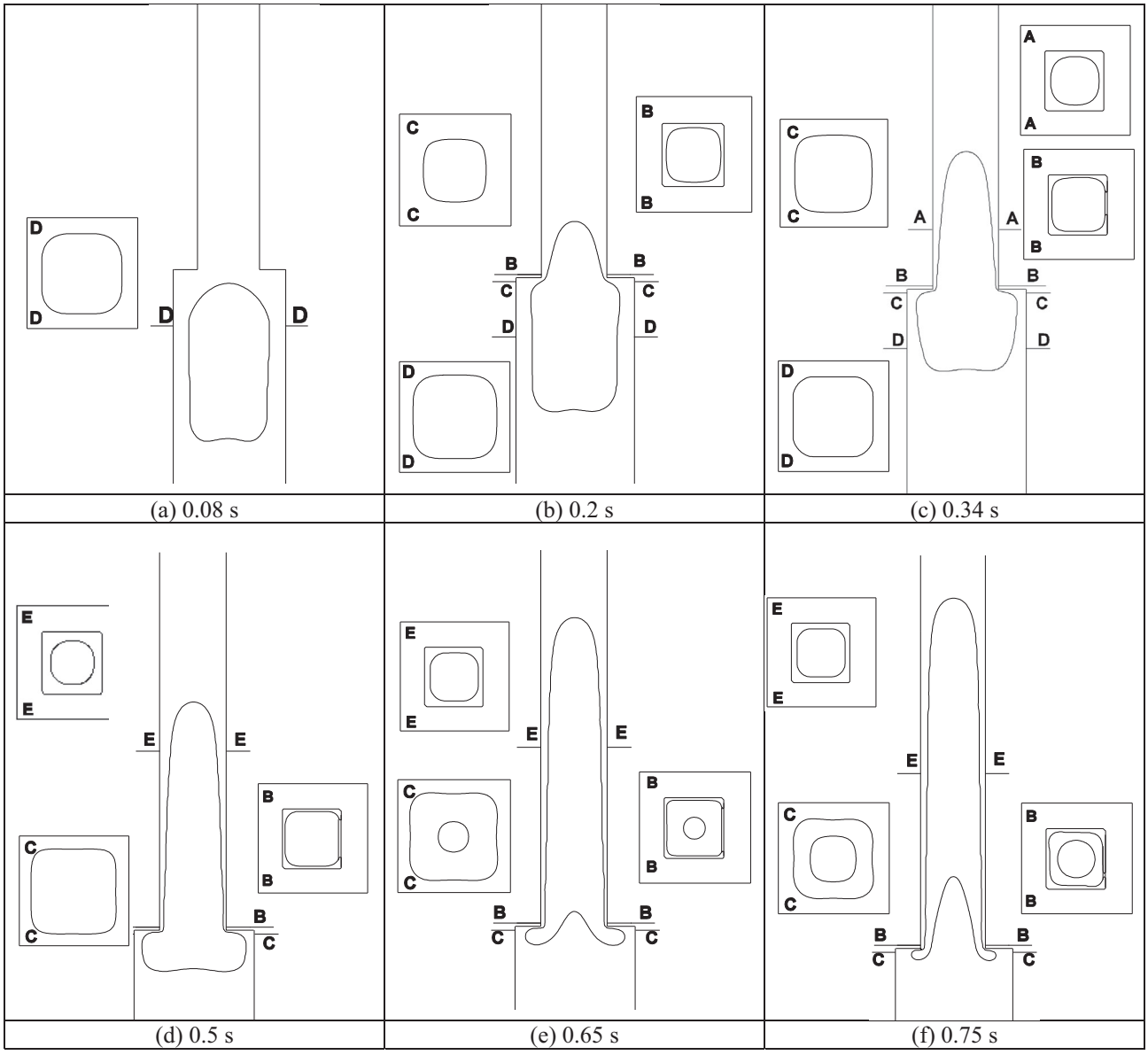

Fig. 8. Phase contours for passage of a long Taylor droplet through symmetric contraction in a vertical channel; droplet becomes slender maintaining symmetry; Lateral view of temporal droplet movement is shown with interface contour at different cross-sectional planes (AA, BB, CC, DD and EE).

be clearly seen (plane CC and DD in Fig. 5(a)) in case of 60° inclined channel as the droplet touches the upper face of its cross-section. Interface of the kerosene droplet also sticks with the upward surface of the conduit in the lower cross-sectional area. It can be clearly observed from section BB and AA of Fig. 5(b), (c). This process continues and gives off-centric rise of Taylor droplet keeping a thick liquid layer at the bottom (Fig. 5(d)). Feed of kerosene above contraction plane retards in this phase showing the possibility of residue.

Fig. 5(e) shows one representative nature of residue formation which has not been seen in case of higher degree inclination with horizontal (Figs. 2 and 3). At 1.85 s, formation of residue completes which is trapped at the contraction plane while slender Taylor droplet with a very long tail creeps up in the smaller cross-sectional channel adhered with the upper side wall. Cross-sectional view FF clearly describes that. Slender tail is also depicted in EE sectional view. With further decrease of the inclination angle from horizontal, volume of residue increases but the movement of droplet becomes quite slow facing less pull of buoyancy. Strong circulation below the droplet is depicted through velocity vectors and streamlines in Fig. 6.

To assess the effect of asymmetry on the evolution of interface during passage through contraction plane, droplet volume present below and above the contraction planes are tracked from numerical simulations for a wide range of inclination of the channel with horizontal. Temporal variations of these volumes for vertical (90°), 75° and 60° inclined channel with horizontal are shown in Fig. 7 which depicts the proceedings of droplet passage through contraction plane. It can be observed that the evolution stage is short (0.7 s) in vertical configuration whereas 60° inclined channel takes almost 2.5 times of span (1.7 s) for completion of passage through contraction plane. Rate of droplet passage through contraction drastically decreases with the shift of the channel from vertical to lean toward horizontal plane. Passage of droplet through inclined channel involves wall adhering interface which creates narrow film for liquid drainage. Resistance to drain liquid through this asymmetric narrow film causes delay in droplet passage. On the other hand, decrease in the magnitude of gravitational pull strength in inclined channels may also lead towards retarded passage.

3.3. Effect of droplet volume on evolution characteristics

Effort has been also made to investigate the pattern of interface evolution while a larger sized kerosene droplet (2 times larger than volume reported in Fig. 2) tries to passage the contraction plane. This scenario is different from the passage of smaller droplet as reported in earlier sections. Here, both in upper and lower sections one can observe area filling nature of kerosene (Fig. 8(c)–(e)) keeping thin water film around. Obtaining higher thickness of water film at the bottom section than the section above contraction plane is quite obvious. In smaller cross-sectional area kerosene droplet behaves like a long, fully developed Taylor droplet which consumes slender body below the contraction plane. It keeps its residue at the corners of the contraction plane for a longer time frame and subsequently transforms into large Taylor droplet.

By the time the residue gets consumed, a crater at the center plane can be observed due to surface tension pull (Fig. 8(f)). Long crater at the tail of the droplet is evident from the strong circulation as shown in Fig. 9.

Effort has been continued to observe the passage pattern for a very long Taylor droplet (4 times larger than volume reported in Fig. 2) through symmetric contraction plane of a vertical channel with the square cross-sectional area. Fig. 10 shows the temporal phase contours for the demonstration of smooth passage around the contraction plane. Interestingly, at this larger volume also daughter kerosene droplets are not produced and the droplet smoothly squeezes itself to accommodate inside the smaller cross-sectional area by increasing its length. As we are dealing with the lower interfacial tension between kerosene and water, surface tension remained passive in this buoyancy dominated rise. This has not allowed neck formation and pinch off at the contraction plane. In the smaller cross-sectional part of the channel, slender droplet has found difficulty in maintaining flat tail and shows bifurcation in the interfacial geometry in terms of water jet (Fig. 10(e), (f)) penetrating through kerosene droplet.

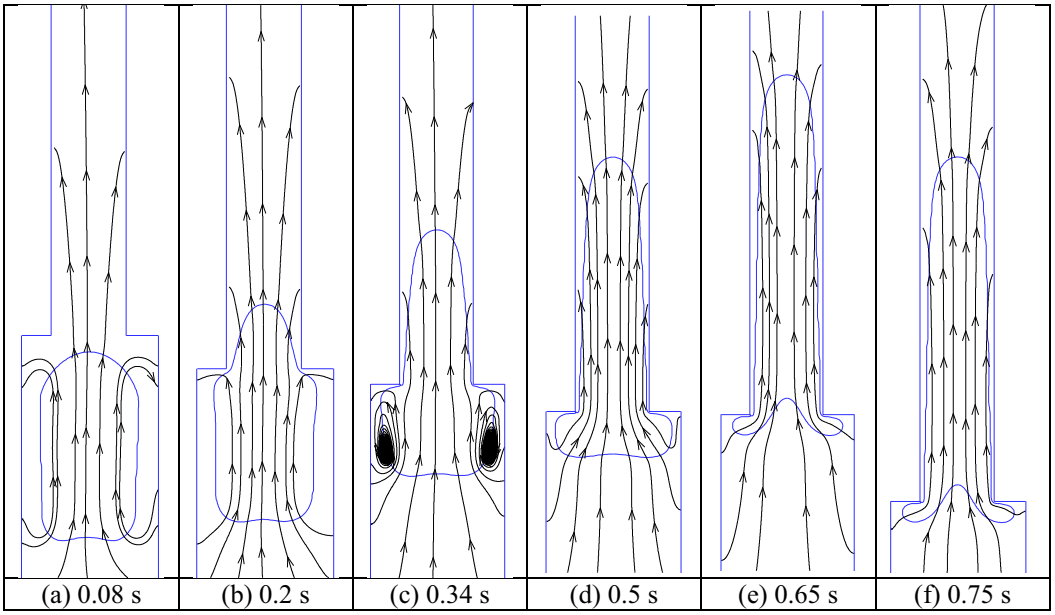

Fig. 9. Change of streamline patterns during passage of a long Taylor droplet through symmetric contraction in a vertical channel; larger circulation cells are characteristics of passage pattern as compared to smaller volumes reported in Fig. 2.

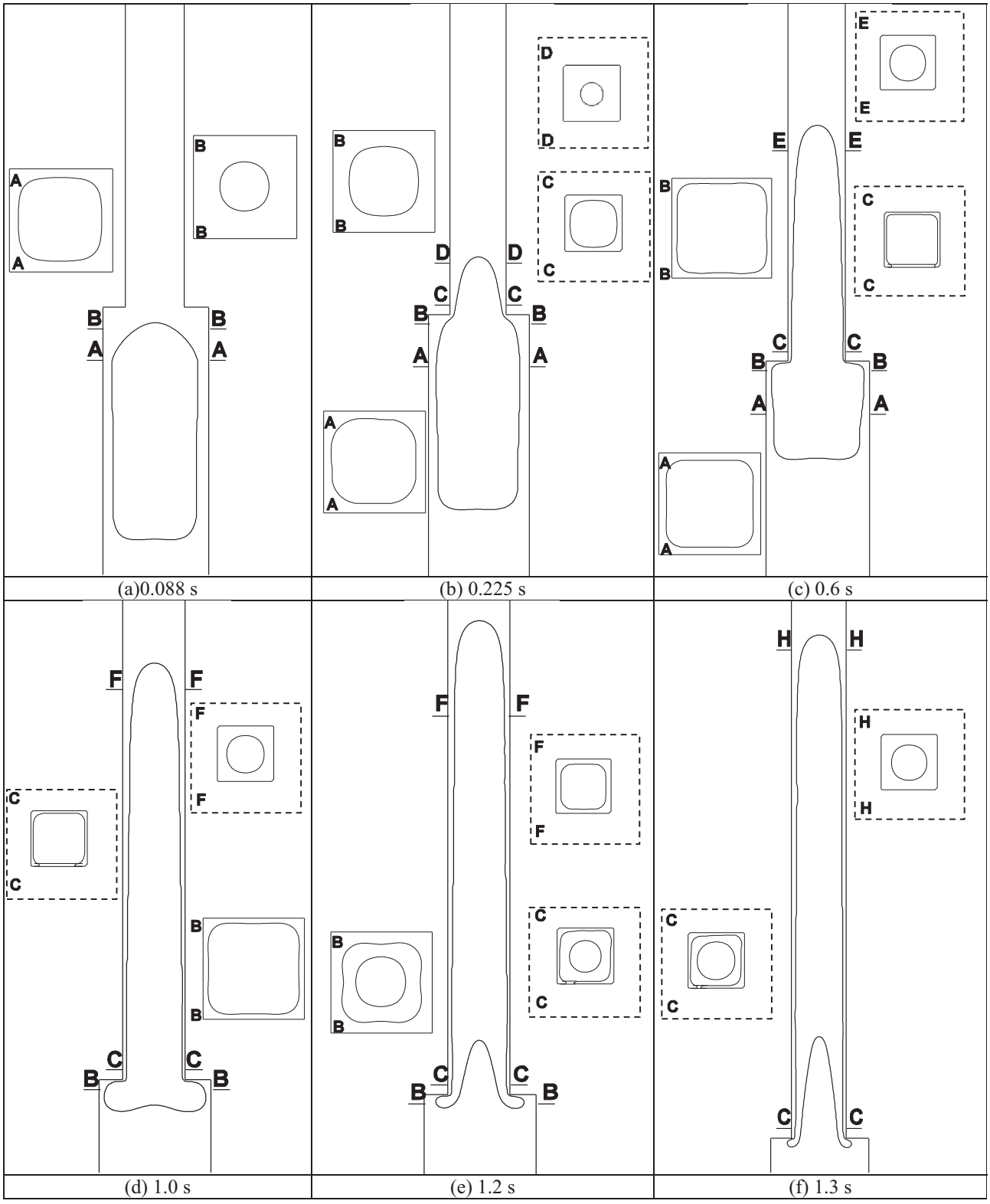

Fig. 10. Passage of a large Taylor droplet through symmetric contraction plane in a vertical channel; cross sectional planes AA, BB, CC, DD, EE, FF and HH clearly demonstrates symmetry even far away from contraction plane.

Aligned streamlines with the channel axis in Fig. 11(a)–(f) clearly demonstrate the dominance of buoyancy force over surface tension. At around 1 s (Fig. 11(d)), strong velocity vectors at the central plane of the channel allows the rush of water which progressively penetrates inside the kerosene droplet to bifurcate its tail. This process continues even after the droplet has completely entered into the smaller cross-sectional area of the channel (Fig. 11(e), (f)).

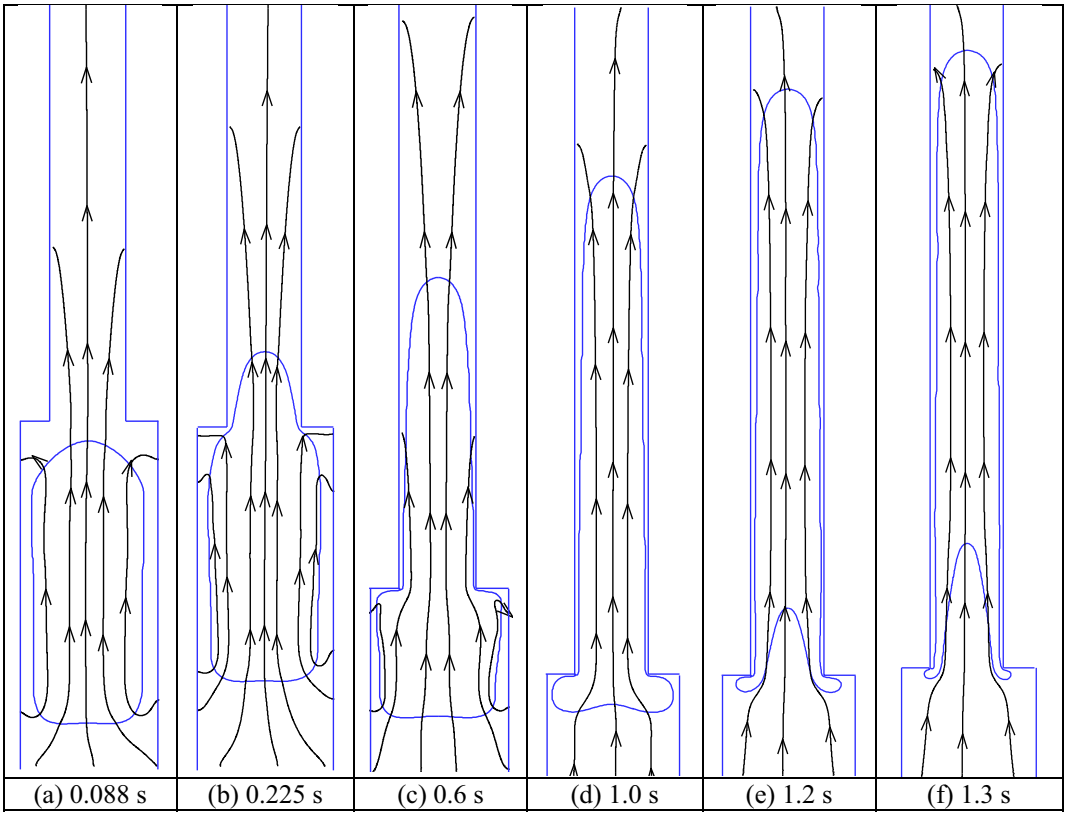

Fig. 11. Streamline patterns during passage of a large Taylor droplet through contraction plane; impingement of water jet has been demonstrated in vertical channel carrying kerosene droplet.

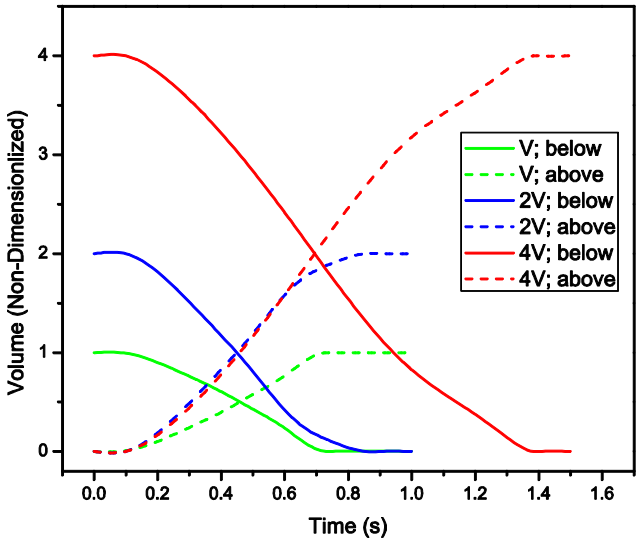

Fig. 12. Volume of kerosene presents above and below the contraction plane for passage of different volumes of droplet in a vertical channel.

A careful comparison of volume account below and above the contraction plane for a wide range of secondary phase volume clearly shows (Fig. 12) that the passage period is lengthier for larger droplets. In comparison to long slender droplets, smaller droplet reorients itself and adjusts the shape promptly. Though it has been found that passage rate is faster in case of larger size droplets, due to its large volume to be passed, the time span for transition gets lengthier than a small droplet. It can be also observed that the passage period doesn't show one to one increasing trend with volume. At higher volume of kerosene droplet, thin film around it above and below the contraction plane delays liquid drainage which helps in droplet passage.

3.4. Kerosene droplet passage through asymmetric contraction of the conduit

After getting the insights of symmetric to symmetric transformation in vertical channels and asymmetric to asymmetric transformation in inclined one, effort has been made to observe the asymmetric evolution of interface from a symmetric one. This has been achieved inside a vertical channel only by offsetting the plane of symmetries of before and after the contraction plane. Here, 3D simulations are performed in order to obtain asymmetric interface only due to offset orientation of contraction plane. Offset between the plane center lines (e) is kept as 1/10th of W_1, side length of cross-sectional area at the bottom. Ratio between W_2 and W_1 has been kept at 0.5 Representative stages of interface evolution are shown in Fig. 13. From the numerical simulation, it can be observed that the droplet behaves symmetrically in both higher and lower cross-sectional area portions. But its asymmetry becomes prompt near the contraction plane. To elaborate that three cross-sectional planes are shown in the form of AA, BB, and CC. At 0.1 s, as the droplet need to passage offset aligned contraction plane, immediate bottom section (CC) and reoriented interface at the upper section (AA) show asymmetrically placed interface as compared to the center plane of the section (Fig. 13(a)). Soon the droplet propagates in the asymmetrically placed lower cross-sectional area and forgets its passage route to generate symmetric

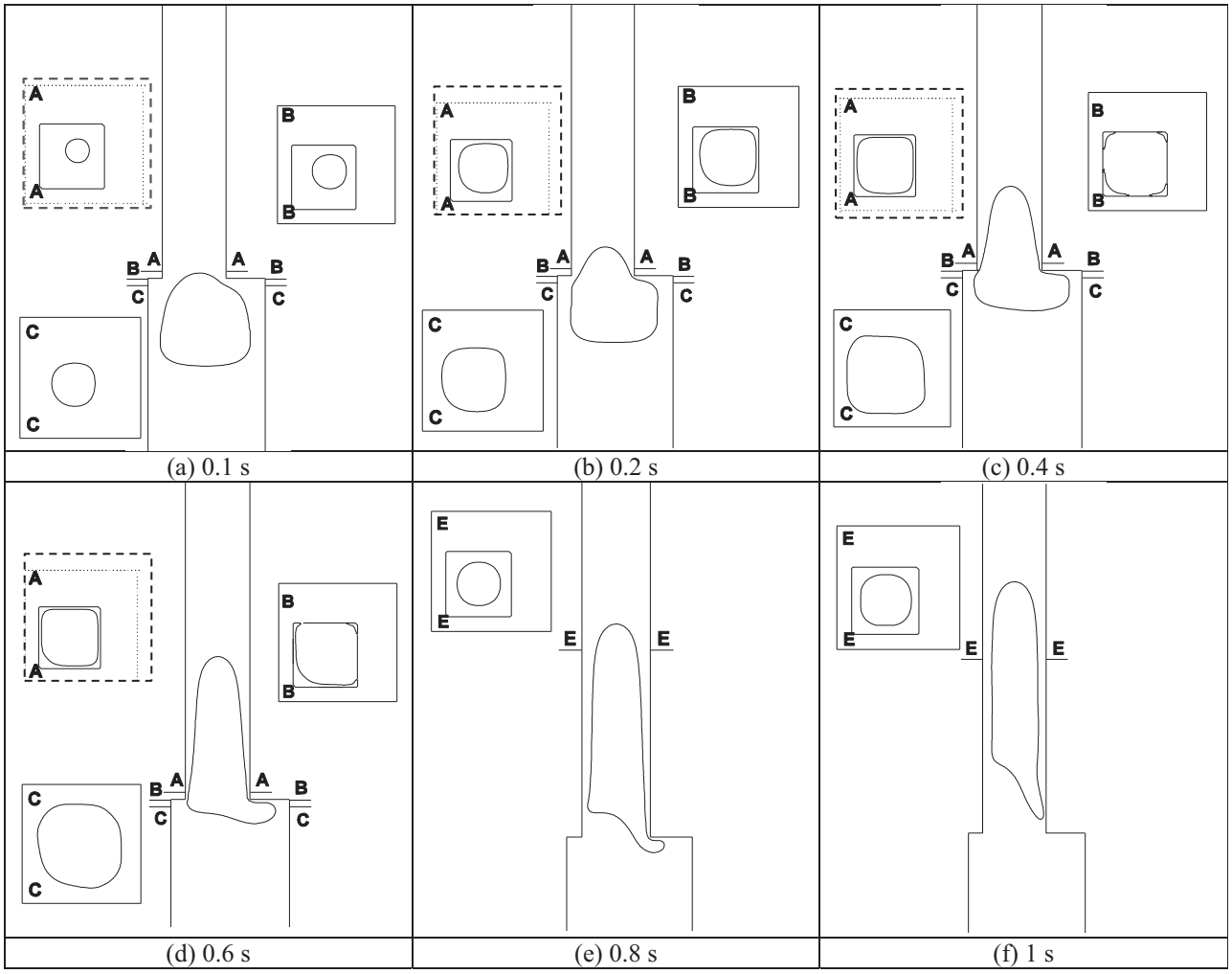

Fig. 13. Pattern of interfacial passage through asymmetric contraction plane in vertical channel; imposed asymmetry in the near plane of contraction but exhibiting symmetry away from the offset contraction plane. Lateral view of temporal droplet movement is shown with interface contour at different cross-sectional planes (AA, BB, CC, DD and EE).

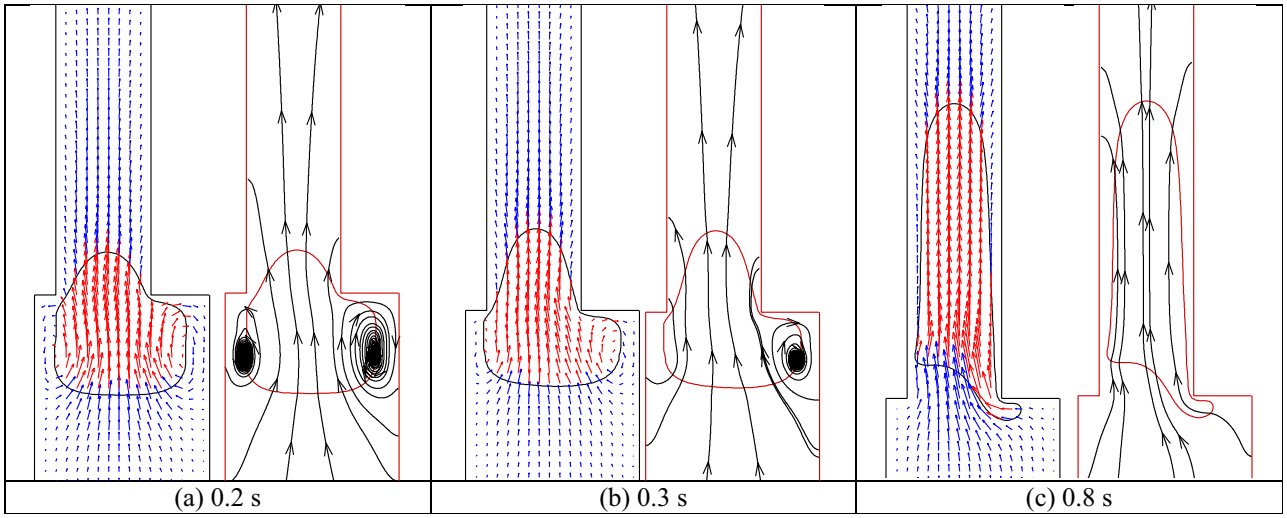

Fig. 14. Demonstration of asymmetry in velocity vectors and streamlines while Taylor droplet passes through a vertical channel with offset contraction plane; asymmetry is only noticed near the contraction plane.

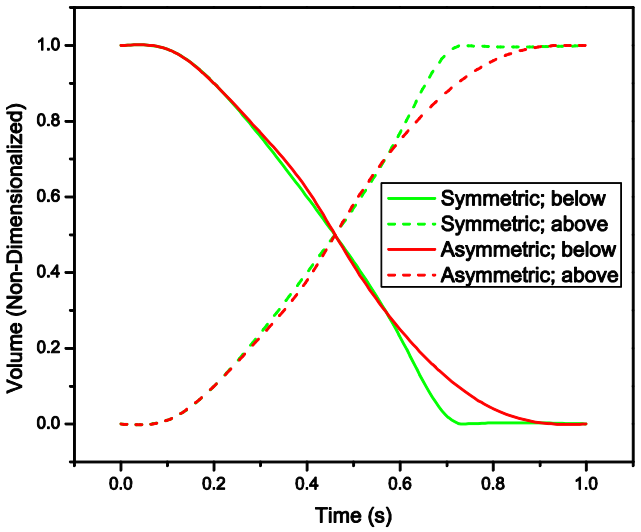

Fig. 15. Volume account of kerosene droplet present above and below the contraction plane for finite and zero offset in symmetry planes; channel is kept as vertical.

configuration (plane AA in Fig. 13(b)–(d)). As the time progresses, larger area occupied by kerosene in plane CC (Fig. 13(b)–(d)) establishes feed from bottom to the top. One can see the asymmetric interfacial configuration in contraction plane (BB) at 0.6 s in Fig. 13(d). After entering into the smaller cross-sectional area, interface moves up as Taylor droplet (Fig. 13(e), (f)). Cross-sectional image EE clearly establishes the symmetric distribution of interface in Fig. 13(e), (f). During passage of Taylor droplet through asymmetric contraction, plane may also lead towards total drainage of liquid near the plane of area reduction, as shown in section BB of Fig. 13(c), (d). A close look at the flow configurations clearly reveals asymmetry only near the contraction zone.

But asymmetry is observable throughout the interface while the droplet passes symmetric contraction inside the inclined channel. In Fig. 14(a), two asymmetric circulation patterns are observed in velocity vectors and streamlines like Fig. 4(a) and Fig. 6(a). But in asymmetric channels, away from the contraction plane streamlines and velocity vectors are parallel to the axial direction, which has been observed in the vertical channel. Similar has not been found out in streamline patterns for the inclined channel having symmetric contraction. Parallel flow becomes evident as the droplet in the smaller channel grows

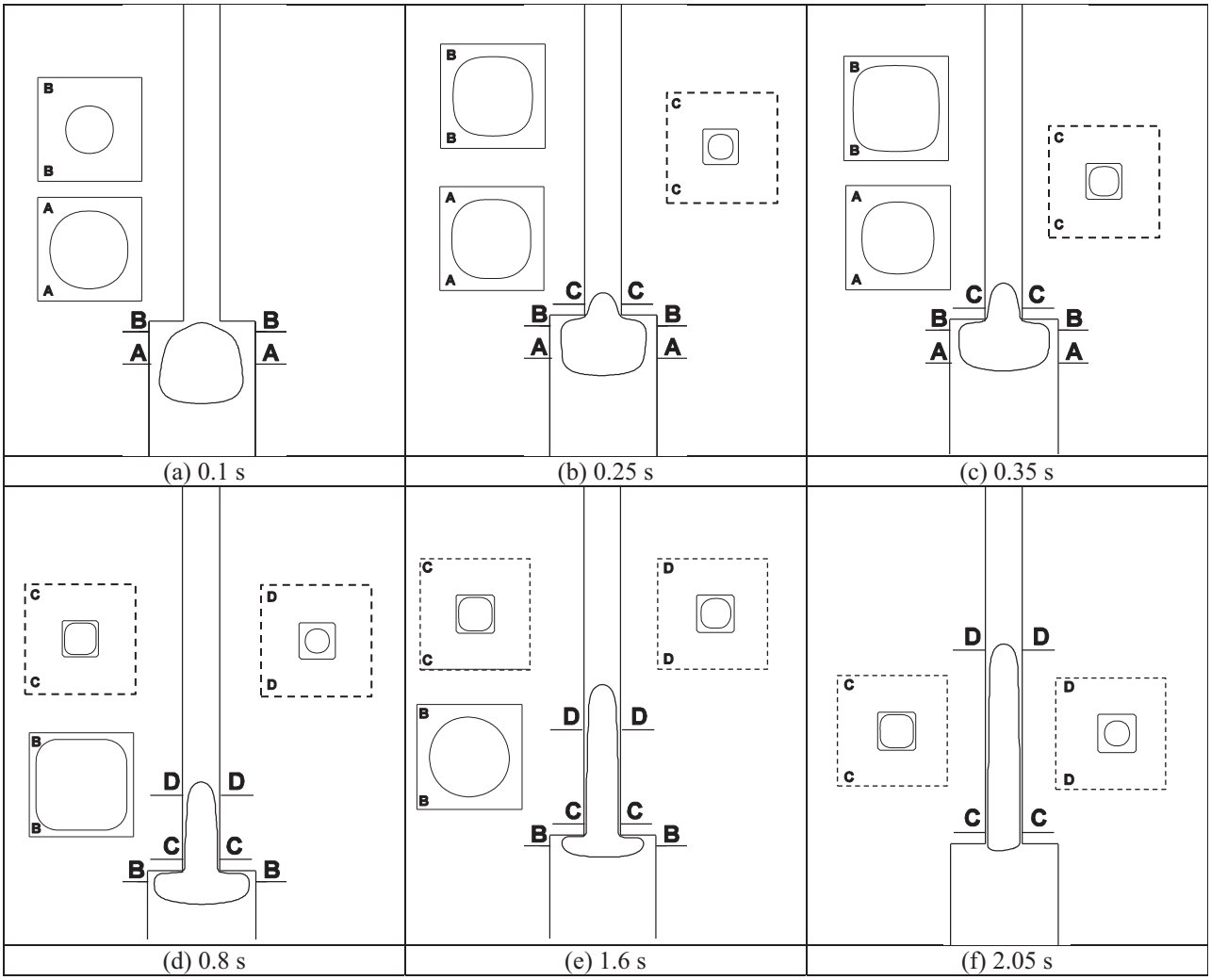

Fig. 16. Stages of interface evolution during passage of a kerosene droplet through narrow (9:100) contraction plane; cross-sectional views demonstrate symmetric nature during passage.

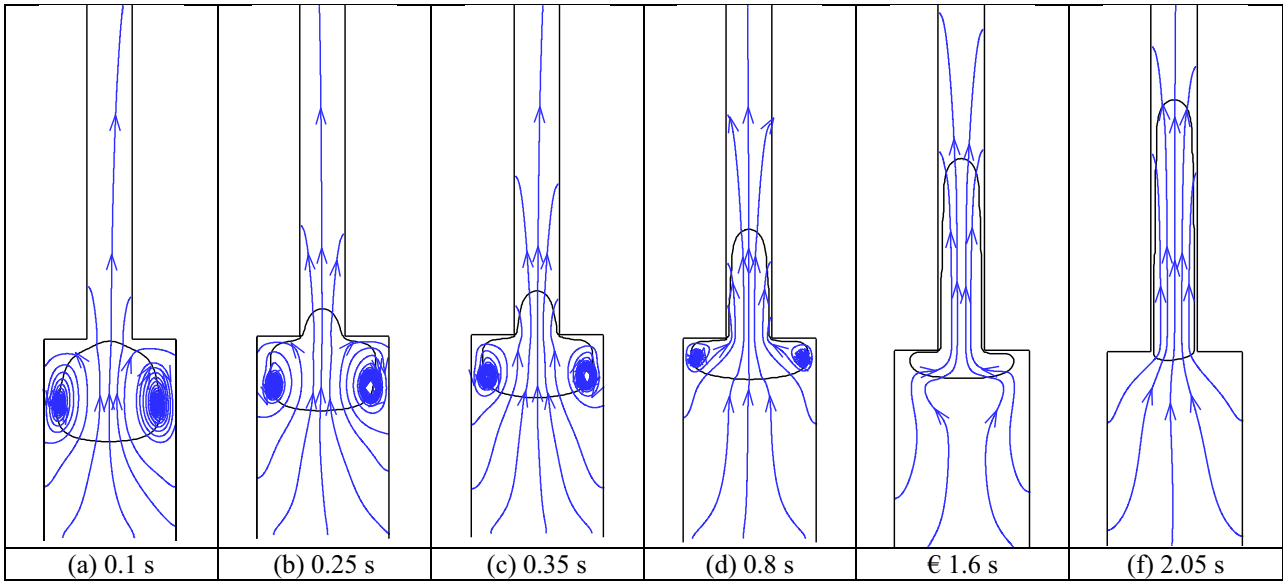

Fig. 17. Change of streamline patterns during passage of a droplet through narrow (9:100) symmetric contraction in a vertical channel; larger circulation cells are characteristics of passage pattern as compared to smaller contraction ratio (1:4), reported in Fig. 2.

further (Fig. 14(b), (c)). Asymmetric circulations are not only different in strength but also vary in size. Area of influence under circulation towards smaller obstruction in the contraction plane is quite smaller than the diametrically opposite plane.

Next, we tried to observe the effect of offset in contraction plane on the rate of passage by plotting the temporal history of volume below and above the plane of area reduction in Fig. 15. It can be clearly observed that the asymmetric contraction plane holds the kerosene droplet for a longer period than the symmetric contraction. Towards the end, droplet passage rate becomes faster in case of symmetric contraction whereas the asymmetric strength of circulation below offset contraction plane retards the passage of residue volume. Such difference in passage span clearly brings out the effect of azimuthal symmetric and wedge shaped azimuthally varying liquid film around the droplet.

3.5. Effect of contraction ratio on evolution characteristics

To understand the effect of contraction extent on shape evolution, simulations are also performed for a symmetric vertical channel with lower contraction ratio than cases reported previously (area contraction 1:4). As representation, $W_2/W_1 = 0.3$ is considered as domain which eventually produce 9:100 area contraction. Phase contours from simulations are plotted in Fig. 16(a)–(f) to demonstrate stages of droplet passage through this steep symmetric contraction. One can see after the initial halt at contraction plane (Fig. 16(a)), orientation of droplet in the lower cross-sectional channel becomes evident. Careful comparison between Fig. 16(b) and Fig. 2(c) establishes slender orientation in the present case. Moreover, liquid film around developing droplet in the lower cross-sectional area is also thin for $W_2/W_1 = 0.3$ than $W_2/W_1 = 0.5$. After obtaining initial protrusion, stages of feeding (Fig. 16(c)–(e)) droplet above contraction plane by residue below proceeds in a similar fashion as shown in Fig. 2 for 1:4 contraction. The droplet elongates along the contraction section and tends to obtain the Taylor droplet shape (Fig. 16(b)–(f)). Comparisons also show that passage takes larger time in 9:100 area contraction channel than 1:4, producing lengthier Taylor droplet after passage. Due to lesser dimension in upper part of the channel, surface tension has not picked up to form a crater at the tail of the Taylor droplet (Fig. 16(f)).

To understand the flow physics behind droplet passing narrow channel, progressive change in streamline pattern is monitored. The formation of circulations near the contraction zone for smaller contraction ratio (Fig. 17(a)–(d)) is more prominent than the larger contraction ratio (Fig. 2(a)–(c)). Though the circulation strength is higher, resistance in droplet passage inside narrow upper portion of the channel increases the passage span. It can be also observed that circulations formed near the contraction zone decrease as the volume of droplet passing through it increases (Fig. 17(a)–(f)).

It has been observed by simulations reported in Figs. 2 and 16, volume flow rate of the droplet will be affected by the contraction ratio (W_2/W_1) of the channel. The droplet is taking more time to pass through the contraction plane as the contraction ratio decreases. The path followed by the volume of droplet passing

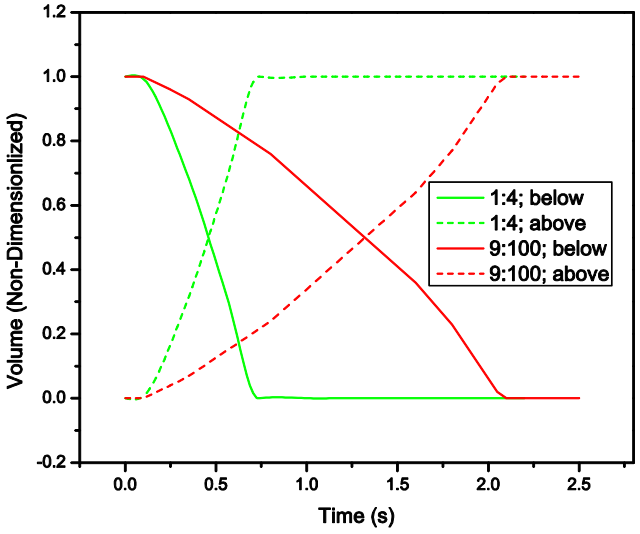

Fig. 18. Volume of droplet passing through the contraction of a vertical channel with different contraction ratios.

through the contraction of a vertical channel is almost similar but with different slope as reported in Fig. 18.

Droplet passage takes approximately 3 times more span in case of 9:100 area contraction ratio than that of 1:4 case. This establishes the effect of resistance given by area contraction on the extent of interface evolution and subsequent span required for passage.

3.6. Passage of a kerosene droplet through orifice

After analysis of interface evolution through the sudden contraction, simulations are also performed to observe the behavior of droplet while passing through a narrow orifice. Here, orifice can be treated as series of sudden contraction and prompt expansion. In gas-liquid medium, researchers (Das et al., 2011) have shown the formation of isolated daughter bubbles as a result of gaseous passage through the orifice. Simulations are performed to observe similar behavior in case of kerosene–water medium with $W_2/W_1 = W_2/W_3 = L/W_1 = 0.3$ (refer to Fig. 1(c)). Phase contours depicting the interfacial shape at different stages of droplet passage through the orifice are plotted in Fig. 19. At the beginning, cap shaped droplet holds at the orifice junction (Fig. 19(a)) and tries to restructure its boundary to squeeze pass the obstruction. It reorients in the contraction part (Fig. 19(b)) in a similar fashion as we have shown in Fig. 16(b). But due to the presence of very small length of contraction region, during its growth, it protrudes in the subsequent expansion region (Fig. 19(c)). Here also kerosene droplet tries to reorients in the unconfined domain and finally obtain spherical shape as the flow of kerosene comes from a linear source from the bottom. One can be observed that the evolution at section CC is confined and on the other hand at section DD is unconfined (Fig. 19(c)). With the progress of time, buoyancy from the bottom supplies continuous flow of kerosene to the pipe section after expansion. This doesn't allow the droplet to grow in size and obtain area filling nature as observed in the bottom portion of the same cross-section. Rather it will elongate (Fig. 19(d)) due to kerosene inertia as jet keeping the cross-sectional area more or less 0.3 times overall area. Kerosene jet increases its length (Fig. 19(e)) by consuming the residue from the bottom of orifice section. At the tip of the jet which faces drag of water, a circular rim is observed as

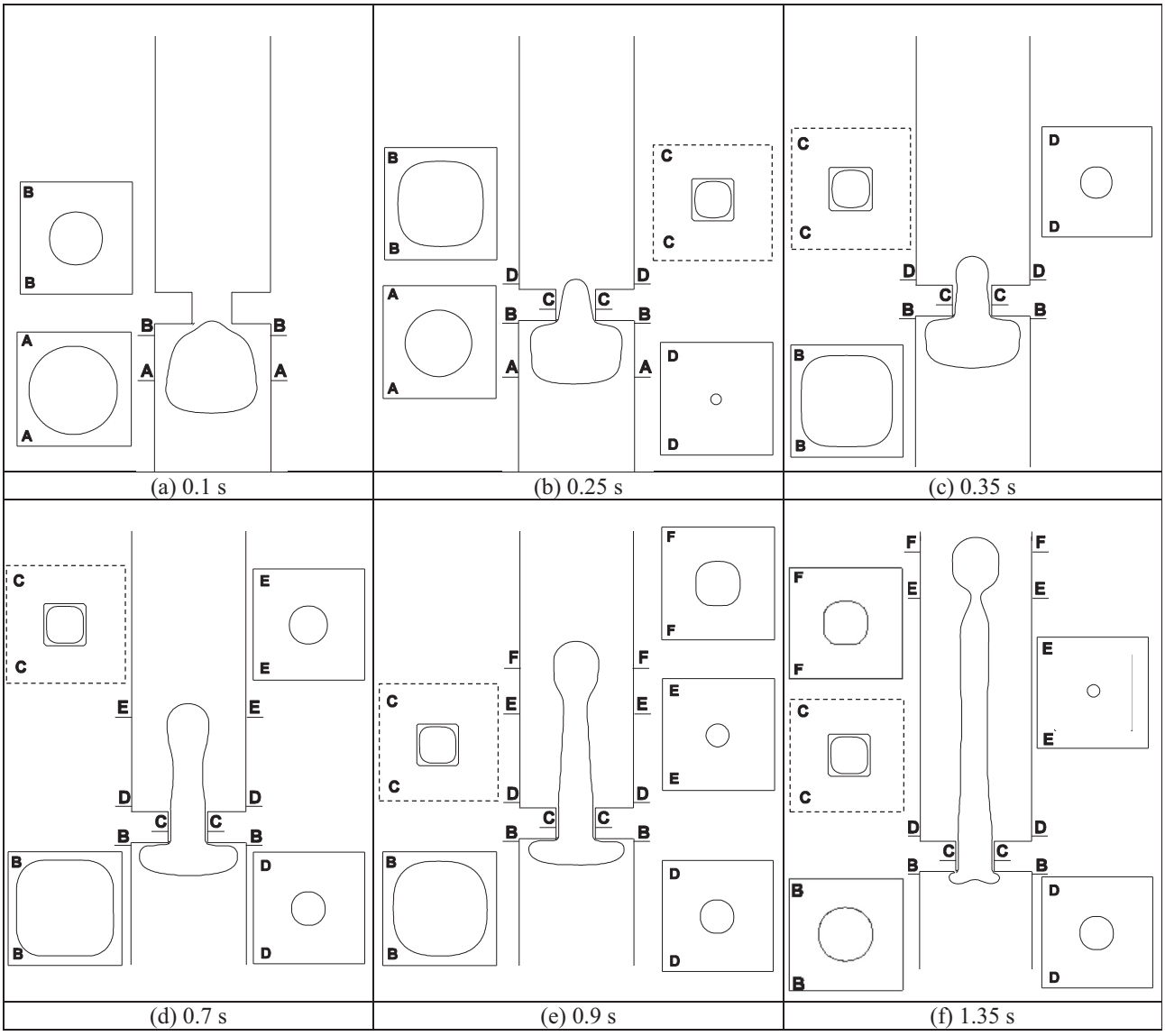

Fig. 19. Stages of interface evolution during passage of a kerosene droplet through narrow (9:100) orifice section; restricted and free protrusion along with slender lamella are the characteristics of interfacial evolution during uprise of a droplet.

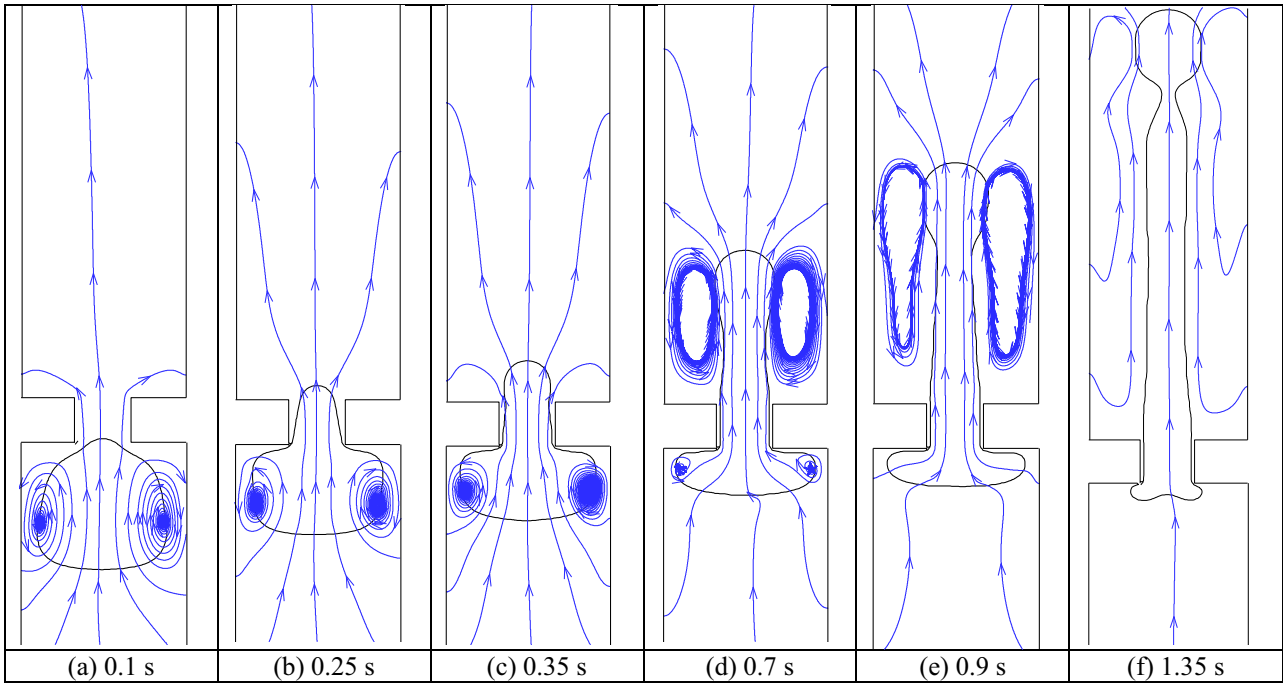

Fig. 20. Pattern of streamlines during passage of a droplet through orifice plane; both upstream and downstream circulations are observed; bottom circulation helps to push the droplet through orifice and upper circulations don't allow it to grow radially.

a result of interfacial tension between liquids. After obtaining almost ten times of length than cross-section and upon full consumption of the bottom inventory slender kerosene lamella continues its uprise in the channel after orifice section. The rim at the tip of the lamella shows the tendency to pinch off for the generation of daughter droplets (Fig. 19(f)). At far downstream of orifice section, the lamella may turn into area filling spherical droplet with preceding smaller daughter droplets.

To understand the flow physics of droplet passage through the orifice, the pattern of streamlines are observed and some representative views are shown in Fig. 20. At the initial stage symmetric circulations are observed (Fig. 20(a)) below the orifice plane which is characteristics of droplet passage through the contraction (Fig. 17 (b)). It is evident that the strength of the circulations below the contraction zone is reduced as the droplet volume present below the contraction is decreased. These strong circulation cells help to propel the kerosene droplet passing the orifice plane. During free evolution above the orifice plane, circulation cells are being observed (Fig. 20(d)) around protruding kerosene jet. The strength and size of circulation increases (Fig. 20(e)) with the growth of jet and restricts its enlargement in cross-sectional direction. Away from the orifice plane circulation cells are not observed (Fig. 20 (f)) which allows surface tension to dominate and produce daughter kerosene droplets.

Next, effort has been made to understand the effect of orifice span (L) on the pattern of interface evolution during the passage of a droplet through it. In Fig. 20, a prompt presence of orifice span has been shown which has not allowed complete consumption of droplet in the restricted domain. To decouple effect of contraction and expansion, simulations are performed with $L = 3W_1 = 6W_2 = 3W_3$. Present situation mimics contraction, stabilization zone, and expansion in series. Phase contours obtained from simulations are shown in Fig. 21 for different stages of droplet passage through restriction of contraction-expansion. In this case, droplet passing contraction zone shows similar behavior which has been observed in Fig. 2. Cap shaped droplet halts at contraction plane (Fig. 21(a)), reorients in the restricted domain (Fig. 21(b)) and consumes its full body to produce a slender Taylor droplet (Fig. 21(c)).

One can notice from cross-sectional images that the Taylor droplet is area filling in nature inside a smaller cross-sectional channel. Upon arriving at the expansion plane, Taylor droplet smoothly enters in the larger cross-sectional channel showing free evolution (Fig. 21(d)). But due to high inertia of Taylor droplet lateral growth has not dominated in comparison to upward elongation. This causes a very minimal change of cross-sectional area of the Taylor droplet (Fig. 21(e)) before and after the expansion. Due to the effect of surface tension at the top of lamella like droplet after expansion, a circular rim is observed (Fig. 21(f)) but that never showed the potential to pinch off. Though the volume of droplet is a big factor over here, but for the observed ranges we have not witnessed pinch off. After entering the expansion zone, lamella like slender droplet faces surface tension and obtains back cap shape in downstream. Hence span of orifice shows huge control for breakage of the droplet while passing a restriction in the flow path comprising contraction and expansion in series.

In order to establish the effect of stabilization zone on transformation of phase contours, streamline patterns in and around the kerosene droplet is shown in Fig. 22. Bottom (Fig. 22(a)) and top (Fig. 22(f)) circulations are observed in a similar fashion that has been shown in Fig. 20. Important features of this simulation are streamlines in the stabilization zone which depicts the parallel nature for free rise of Taylor droplet. Pattern of these parallel streamlines (Fig. 22(c)–(e)) has not allowed upper circulations to grow with time causing pinch off.

4. Conclusion

Lattice based numerical simulations are performed for obtaining evolution of liquid-liquid interface during passage through restrictions. Symmetric and Asymmetric contractions are tried as

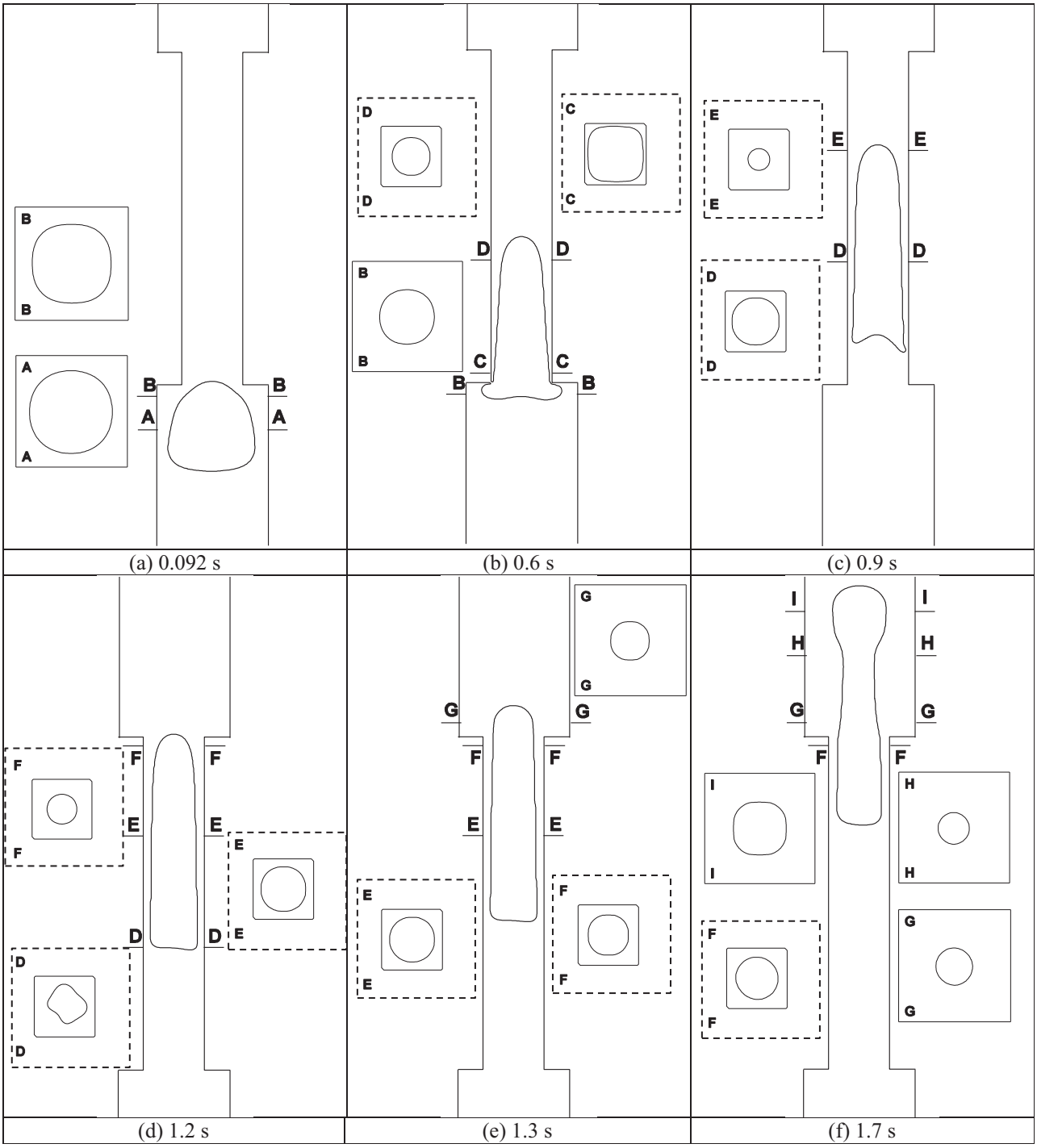

Fig. 21. Phase contours for different stages of droplet passage around restrictions in flow path inside a channel; contraction, stabilization zone and expansion are the characteristics of restriction; generation of daughter droplet is not observed due to presence of stabilizing zone.

a restriction in the domain for a wide range of contraction ratio, droplet volume, inclination and offset. Symmetric contraction in vertical channel showed smooth passage of interface with a line of symmetry. In downstream of contraction, area filling nature of droplet is lost and lengthy lamella like interface has been observed. Decrease in contraction ratio has resulted in the increase of resistance to passage and produces lengthier droplet. Asymmetric circulations are observed to be the reason behind upward shift of the interface creating wedge shaped water film around the droplet. Offset of contraction plane showed asymmetry interface and streamlines only near the plane of area reduction. Simulations also performed to observe the droplet passage through the orifice having almost zero stabilization zone between contraction and expansion. Above the contraction plane, it can be observed that the interface evolution of kerosene droplet has been restricted which is similar to the results of simple contraction simulations. Strong circulations around the droplet in expansion zone don't allow radial increase of kerosene cross-section at larger area part of the channel. Away from the orifice plane, due to surface tension, kerosene droplet pinches off and produces a daughter droplet. Simulations with prolonged stabilization zone showed decrease in the tendency of interface fragmentation and droplet bifurcation.

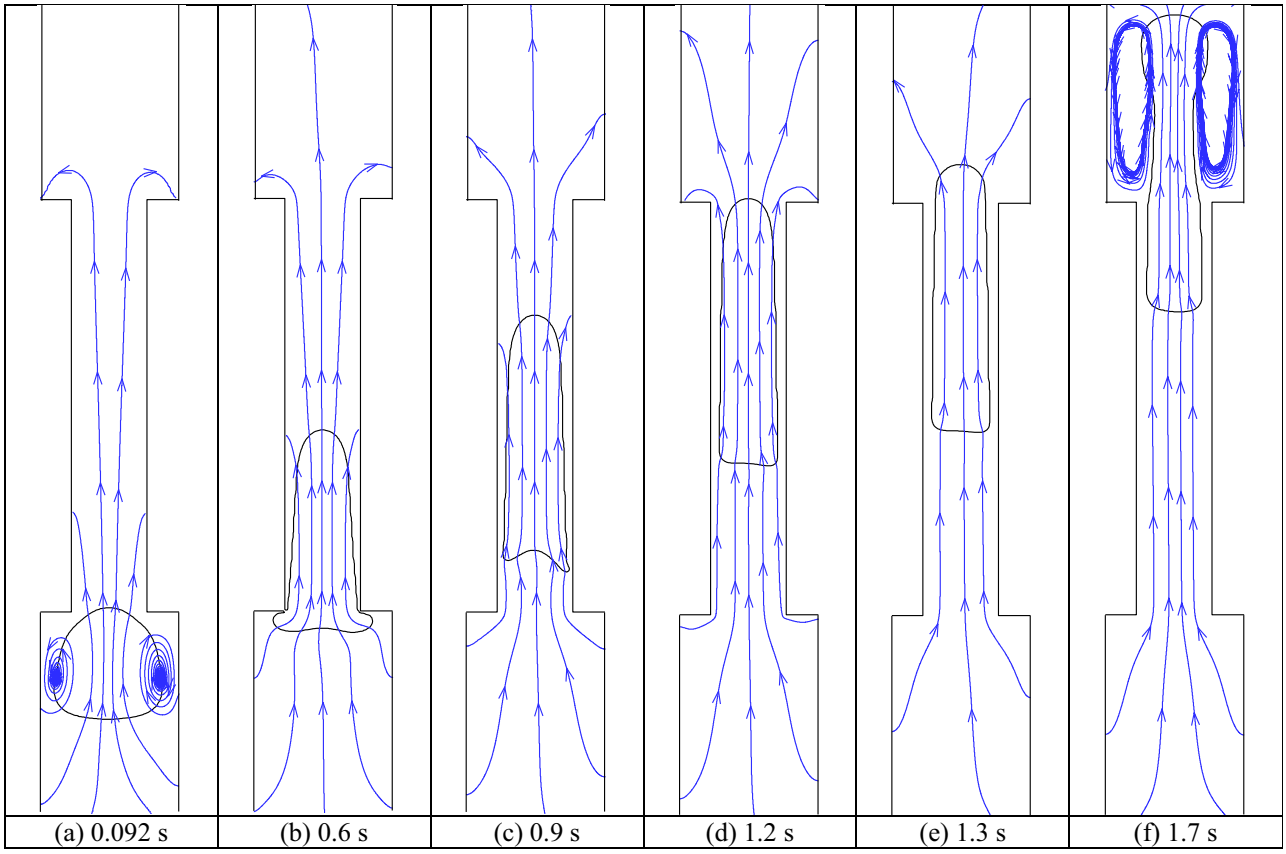

Fig. 22. Pattern of streamlines in different stages of droplet passage around restriction comprising contraction, stabilization zone and expansion; parallel streamlines in droplet passing through stabilization zone establishes reason behind smooth entry after expansion.

Acknowledgment

TS wants to acknowledge support of National Institute of Technology Uttarakhand, India for performing research as a part-time scholar of IIT Roorkee, India.

References

Abdelall, F.F., Hahn, G., Ghiaasiaan, S.M., Abdel-Khalik, S.I., Jeter, S.S., Yoda, M., Sadowski, D.L., 2005. Pressure drop caused by abrupt flow area changes in small channels. Exp. Therm. Fluid Sci. 29 (4), 425–434.

Aslan, E., Taymaz, I., Benim, A.C., 2014. Investigation of the lattice Boltzmann SRT and MRT stability for lid driven cavity flow. Int. J. Mater., Mech. Manuf. 2 (4), 317–324.

Attou, A., Giot, M., Seynhaeve, J.M., 1997. Modelling of steady-state two-phase bubbly flow through a sudden enlargement. Int. J. Heat Mass Transfer 40 (14), 3375–3385.

Balakhrisna, T., Ghosh, S., Das, G., Das, P.K., 2010. Oil–water flows through sudden contraction and expansion in a horizontal pipe–phase distribution and pressure drop. Int. J. Multiphase Flow 36 (1), 13–24.

Bhusan, S., Ghosh, S., Das, G., Das, P.K., 2009. Rise of Taylor bubbles through narrow rectangular channels. Chem. Eng. J. 155 (1), 326–332.

Chen, Y., Chu, M.C., Liaw, J.S., Wang, C.C., 2008. Two-phase flow characteristics across sudden contraction in small rectangular channels. Exp. Therm. Fluid Sci. 32 (8), 1609–1619.

Chisholm, D., 1968. Predicting of pressure losses at changes of section, bends and throttling Devices. NEL Report. 388.

Das, A.K., Das, P.K., 2010. Multimode dynamics of a liquid drop over an inclined surface with a wettability gradient. Langmuir 26 (12), 9547–9555.

Das, A.K., Das, P.K., Saha, P., 2011. Formation of bubbles at submerged orifices – experimental investigation and theoretical prediction. Exp. Therm. Fluid Sci. 35 (4), 618–627.

Geiger, G.E., 1964. Sudden contraction losses in single and two-phase flow. University of Pittsburgh, Pittsburgh, USA.

Ghosh, S., Patil, P., Mishra, S.C., Das, A.K., Das, P.K., 2012. 3-D lattice Boltzmann model for asymmetric Taylor bubble and Taylor drop in inclined channel. Eng. Appl. Comput. Fluid Mech. 6 (3), 383–394.

Gnglielmini, G., Lorenzi, A., Muzzio, A,. Sotgia, G., 1986. Two-phase flow pressure drops across sudden area contractions pressure and void fraction profiles. In: Proc. 8th Int. Heat Transfer Conf.; vol. 5, pp. 2361–2366.

Janssen, E., Kervinen, J.A., 1964. Two-phase pressure drop across contractions and expansions water-steam mixtures at 600 to 1400 psia. No. GEAP-4622. General Electric Co. Atomic Power Equipment Dept., San Jose, Calif.

Kawahara, A., Mansour, M.H., Sadatomi, M., Law, W.Z., Kurihara, H., Kusumaningsih, H., 2015. Characteristics of gas–liquid two-phase flows through a sudden contraction in rectangular microchannels. Exp. Therm. Fluid Sci. 66, 243–253.

Mandal, T.K., Das, G., Das, P.K., 2008. Motion of Taylor bubbles and Taylor drops in liquid–liquid systems. Ind. Eng. Chem. Res. 47 (18), 7048–7057.

Meng, J., Xiao-Jun, G., Emerson, D.R., 2018. Analysis of non-physical slip velocity in lattice Boltzmann simulations using the bounce-back scheme, Journal of Computational Sciences, In Press http://doi.org/10.1016/j.jocs.2017.10.008.

Miqdad, A.M., Datta, S., Das, A.K., Das, P.K., 2016. Effect of electrostatic incitation on the wetting mode of a nano-drop over a pillar-arrayed surface. RSC Adv. 6 (111), 110127–110133.

Padilla, M., Revellin, R., Bonjour, J., 2013. Two-phase flow of HFO-1234yf, R-134a and R-410A in sudden contractions: visualization, pressure drop measurements and new prediction method. Exp. Therm. Fluid Sci. 47, 186–205.

Sadatomi, M., Miyagawal, S., Santoso, B., Kawahara, A., 2013. Air-water two-phase flow through U-bend, sudden expansion and sudden contraction in rectangular mini-channels. Comput. Methods Multiphase Flow VII 79, 63.

Schmidt, J., Friedel, L., 1997. Two-phase pressure drop across sudden contractions in duct areas. Int. J. Multiphase Flow 23 (2), 283–299.

Succi, S., d'Humieres, D., Qian, Y.H., Orszag, S.A., 1993. On the small-scale dynamical behavior of lattice BGK and lattice Boltzmann schemes. J. Sci. Comput. 8 (3), 219–230.

Weisman, J., Hussain, A., Harshe, B., 1976. Two phase pressure drop across abrupt area changes and restrictions. In: Proc. Two-Phase and Heat Transfer Symposium, Hemisphere, Washington, DC, pp. 301–303.

Yu, Z., Fan, L.S., 2010. Multirelaxation-time interaction-potential-based lattice Boltzmann model for two-phase flow. Phys. Rev. E 82, (4) 046708.

Zheng, H.W., Shu, C., Chew, Y.T., 2006. A lattice Boltzmann model for multiphase flows with large density ratio. J. Comput. Phys. 218 (1), 353–371.

Zou, Q., He, X., 1997. On pressure and velocity boundary conditions for the lattice Boltzmann BGK model. Phys. Fluids 9 (6), 1591–1598.